Development of the Direct-Estimation Albedo Algorithm for Snow-Free Landsat TM Albedo Retrievals Using Field Flux Measurements

Xiaoning Zhang, Ziti Jiao, Yadong Dong, Tao He, Anxin Ding, Siyang Yin, Hu Zhang, Lei Cui, Yaxuan Chang, Jing Guo, and Rui Xie

Abstract—Anisotropy information from moderate-to-coarse-resolution sensors [e.g., 500-m Moderate Resolution Imaging Spectroradiometer (MODIS)] is widely applied to estimate high-resolution surface albedo. Simulated albedos using MODIS bidirectional reflectance distribution function (BRDF) parameters as prior knowledge based on the kernel-driven model are employed to build and assess the lookup table (LUT) of the direct-estimation method, which is then used to estimate high-resolution albedos directly from top-of-atmosphere (TOA) reflectance data (e.g., Landsat albedo). Previously, the errors in the simulated albedos were not considered in building and assessing the LUT. In this article, daytime time-series (30 min) of snow-free albedo measurements with sufficient solar zenith angles (SZAs) were introduced to build the LUT for snow-free Landsat TM surface shortwave broadband albedo (TM albedo) retrievals, together with TOA-simulated reflectance by concurrent daily MODIS BRDF parameters. The assessment utilizes an independent data set and shows larger discrepancies between the estimated and measured albedos [root-mean-square errors (RMSEs) of >0.03 at SZAs ≥ 60°] than those in previous articles. To reduce inconsistencies between the MODIS BRDF parameters and the observed albedos, as well as possible spatial resolution differences between the MODIS and Landsat data, we adopted a correction strategy that first linearly adjusts the MODIS BRDF parameters to match the albedo measurements by a magnitude method, and second, the TOA reflectance simulations were further corrected by concurrent TM reflectances. The developed algorithm shows a significant improvement after using such corrections as *a priori* (RMSE < 0.02 at SZA ≤ 75°). The validation indicates improved accuracies in the TM albedo estimation. These improvements may provide potential albedo estimations for nadir-viewing high-resolution sensors using coarse-resolution anisotropy information.

Index Terms—Accuracy assessment, daytime time-series flux measurements, direct-estimation albedo method, two-step correction strategy.

X. Zhang is with the State Key Laboratory of Remote Sensing Science, Jointly Sponsored by Beijing Normal University and Institute of Remote Sensing and Digital Earth, Chinese Academy of Sciences, Beijing 100875, China, with the Beijing Engineering Research Center for Global Land Remote Sensing Products, Faculty of Geographical Science, Institute of Remote Sensing Science and Engineering, Beijing Normal University, Beijing 100875, China, and also with the Unmanned Aerial Vehicle Systems Engineering Institute, China Aerospace Science and Technology Corporation, Beijing 100094, China.

Z. Jiao, A. Ding, S. Yin, L. Cui, Y. Chang, J. Guo, and R. Xie are with the State Key Laboratory of Remote Sensing Science, Jointly Sponsored by Beijing Normal University and Institute of Remote Sensing and Digital Earth, Chinese Academy of Sciences, Beijing 100875, China, and also with the Beijing Engineering Research Center for Global Land Remote Sensing Products, Faculty of Geographical Science, Institute of Remote Sensing Science and Engineering, Beijing Normal University, Beijing 100875, China (e-mail: jiaozt@bnu.edu.cn).

Y. Dong is with the State Key Laboratory of Remote Sensing Science, Beijing 100875, China.

T. He is with the School of Remote Sensing and Information Engineering, Wuhan University, Wuhan 430079, China, and also with the Department of Geographical Sciences, University of Maryland, College Park, MD 20742 USA.

H. Zhang is with the School of Geographic and Environmental Sciences, Tianjin Normal University, Tianjin 300387, China.

Color versions of one or more of the figures in this article are available online at http://ieeexplore.ieee.org.

Digital Object Identifier 10.1109/TGRS.2019.2946598

I. INTRODUCTION

SURFACE albedo is recognized as an important factor in climate change monitoring [1], where the surface albedo is defined as the ratio of the reflected radiative flux in the viewing hemisphere to the total incident flux [2]. Due to the frequent sensor revisits at coarse spatial resolutions, multiangle reflectances can be collected over a short period [3], which are then used to describe surface reflectance anisotropy based on various models, such as the widely used semiempirical kernel-driven bidirectional reflectance distribution function (BRDF) model [4], [5]. Thus, albedo can be calculated as the bihemispherical integral of the BRDF from viewing and solar geometries, such as the operational 500-m albedo products of the Moderate Resolution Imaging Spectroradiometer (MODIS) based on the Ross-Thick-Li-Sparse-Reciprocal (RTLSR) model [6]. In addition, the 1-km SPOT/VEGETATION surface albedo product (GEOV1 albedo) [7], [8] is generated by using the Roujean model [4]. The surface albedo can also be retrieved by linking different BRDF models [9], [10].

Albedo products at fine spatial resolutions are in high demand, as fine spatial resolution can aid in describing subtle albedo changes and can be utilized to validate albedo products at coarse resolutions [11]. However, BRDF samplings are rarely sufficient, particularly for high-resolution satellite sensors, and thus, prior BRDF information is usually helpful

for describing land surface anisotropy at fine spatial resolutions [12]–[15]. By applying MODIS BRDF data as prior knowledge, various methods have been developed to calculate albedo at high spatial resolutions.

Various efforts have been made to estimate the surface albedo from surface reflectance data. A general method for albedo determination consists of separate processing chains: atmospheric correction, directional reflectance normalization, spectral albedo calculation, and narrowband-to-broadband albedo conversion. The 6SV radiative transfer code is mainly used to perform atmospheric correction, by which surface reflectances can be obtained from top-of-atmosphere (TOA) reflectances for Landsat TM, ETM+, and OLI data [16]. For 30-m Landsat pixels that are homogeneous within the corresponding 500-m MODIS spatial scale, the ratio of nadir reflectance to albedo at the MODIS pixel is applied to the Landsat scale for albedo estimation [14], [17], and the method is being used to develop a Landsat-8 surface albedo algorithm for determining Landsat albedos [18]. In terms of heterogeneous land surfaces, BRDF shapes for MODIS pixels as functions of the normalized difference vegetation index (NDVI) and land cover composition of subpixels are used as prior information to interpret the reflectance anisotropy at the Landsat scale [13], [19], [20]. Notably, for these methods, an accurate atmospheric correction from the initial satellite signal above the TOA is required to obtain reliable surface reflectances [16]. In addition, although airborne and ground-based multiangle observations can also aid in obtaining surface albedos at fine resolutions, these observations are limited to small regions depending on the well-designed experiments acquiring sufficient multiangle reflectances [15], [21].

Another alternative method is to perform the estimation directly from the TOA reflectance data. Recently, the direct-estimation albedo approach has been successfully applied to estimating albedo at fine resolutions, such as the 30-m Chinese HuanJing (HJ) Satellite [22] and a series of sensors onboard Landsat [23], which follows the theory of retrieving surface albedo directly from TOA reflectance, as proposed by Liang [24] and Liang *et al.* [25]. The method has been used to estimate albedos for the 1–5-km Global LAnd Surface Satellite (GLASS) data set [26], [27] and to estimate daily albedos for the Visible Infrared Imaging Radiometer Suite (VIIRS) sensor [28]–[30]. The key task is to build a regression lookup table (LUT) of TOA spectral reflectances and surface albedos in sun-view geometries, including the solar zenith angle (SZA), view zenith angle (VZA), and relative azimuth angle (RAA), where the MODIS BRDF information and atmospheric radiative transfer process are considered in advance when building the LUT. Using the LUT, surface albedos can be easily estimated from TOA reflectances. Thus, the possible errors resulting from the atmospheric correction can be avoided, especially for sensors onboard the Landsat platform prior to Landsat 8 due to the lack of accurate aerosol loadings [31].

Currently, MODIS albedos that are fully simulated by using MODIS BRDF parameters based on the kernel-driven model are used to build and assess the regression LUT of the direct-estimation albedo algorithm [22]–[24], [28]; therefore, the accuracy of the method mainly relies on the MODIS BRDF/albedo product. However, the product shows an overall accuracy of albedo estimation that is within a 0.05 root-mean-square error (RMSE) with increasing errors as SZA increases [32]–[34], and accuracies occurring near the local solar noon overpass time are higher than those of other times during the day [33]. Consequently, these errors originating from MODIS BRDF data may transfer to the final regression LUT. In addition, although MODIS BRDF data have been directly used in the Landsat TM nadir reflectance for various applications [14], [23], [35], the potential scale difference in BRDF shapes between the two sensors may also be a major source of uncertainty in these applications [36]–[38].

In fact, numerous upwelling/downwelling radiative flux measurements at sites worldwide are available [13], [23], [26], [34], and the albedo ratios are promising to replace the simulated MODIS albedos in the direct-estimation method, which will most likely reduce the uncertainties caused by relying on only albedo simulations. When building the regression LUT for multiangle sensors such as MODIS and VIIRS as well as Chinese HJ satellite [22], [24], [26], [28], [30], directional reflectances at three orientations (SZA, VZA, and RAA) are needed. Notably, nadir directional reflectances at a certain SZA are invariant for arbitrary azimuth angles [35], and this peculiarity means that the LUT for near-nadir sensors, such as Landsat [23], is related to only the SZA rather than all three angles. Therefore, these time-series albedo measurements with a wide range of SZAs can be utilized to build and assess the LUT of the direct-estimation method for nadir view sensors, in conjunction with the concurrent daily Collection V006 MODIS BRDF product [32], [39], [40] to simulate TOA reflectances. In addition, these concurrent albedo measurements and TOA reflectance observations can aid in further reducing uncertainties in the direct-estimation method, which result from data inconsistencies and scale differences between MODIS and Landsat.

In this article, using the advantages of frequent radiative flux measurements at global sites, time-series snow-free shortwave broadband albedo measurements were first used to build and assess the regression LUT of the direct-estimation albedo algorithm for the 30-m Landsat TM data. In addition, we propose a correction strategy to reduce the errors caused by the potential inconsistencies between the MODIS BRDF parameters and the observed albedos and the spatial differences between MODIS and TM. In Section II, the data set used in this article is introduced. Then, the experimental design and methods are illustrated in Section III. We analyze the accuracy of these regression LUTs before and after using such a correction strategy based on the assessment and validation results presented in Section IV. Finally, some new findings and plans for future work are summarized in Section V.

II. DATA AND PREPROCESSING

A. Flux Measurements at 47 Sites

Time-series snow-free flux measurements at 47 sites for multiple years were collected, as shown in Fig. 1 and Table I; these sites are located in many countries. Among the data
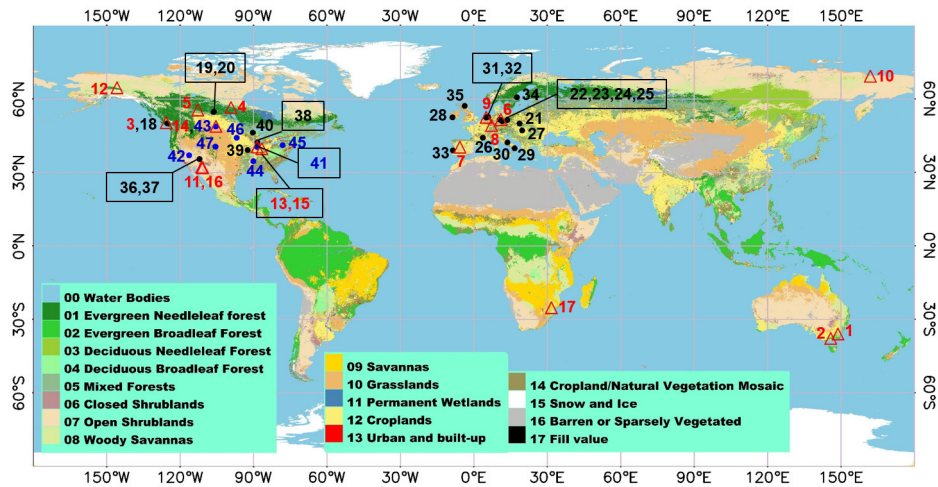
Fig. 1.   Distribution of the 47 sites that are listed in Table I. Sites 1–17, 18–40, and 41–47 are shown as red triangles, black dots, and blue dots, respectively.

set, data from sites 1–40 were acquired from the FLUXNET (http://fluxnet.fluxdata.org/) and AmeriFlux (http://ameriflux.lbl.gov/) networks, and these sites were demonstrated to be homogeneous and thus have a representativeness at the 500-m spatial scale for the period of 2000–2007 [26], [41]. The downwelling/upwelling shortwave radiative flux data (280–2800 nm) are recorded every 30 min for the first 40 sites, except for sites 1 and 15, which both have a temporal resolution of 1 h [41]. In addition, the seven widely used sites in the surface radiation (SURFRAD) network were also included (http://www.esrl.noaa.gov/gmd/grad/surfrad/index.html) [13], [14], [23], [34], where the radiative measurements (280–3000 nm) are released at 3- and 1-min intervals before and after 2009, respectively. The shortwave broadband albedo can be calculated as the ratio of the upwelling portion to the total downwelling shortwave solar radiation. The corresponding SZAs can be determined based on the measuring time and geographic location. The circular footprint diameters ($f[m]$) of these flux measurements were calculated based on the relationships between the tower height above the canopy ($H[m]$) and half of the field of view (HFOV[degree(°)]) of the pyranometers [i.e., $f = 2H \tan(\text{HFOV}°)$] [13], [41]. Notably, a value of 81° was used as a general effective HFOV [32]. Finally, the averaged albedo estimations of the corresponding TM pixels within the footprint of each site were used for algorithm validation, which was compared with the average measured albedos within ±30 min of the Landsat overpass time.

The regression LUT for the Landsat TM data is a function of the SZA, and therefore, we need sufficient SZAs as well as albedos to build the LUT. In previous studies, surface albedos for SZAs of 0°–70° at a 5° interval have been commonly simulated [22], [23]. Regression coefficients are stored in the LUT for these SZAs, and the final albedo for a specific SZA is calculated via a linear interpolation of the estimated albedos at the two nearest SZAs. The data set from the first 17 sites for 2004 and 2005 was selected to build and assess the regression LUT of the direct-estimation

algorithm, as shown in Fig. 1 (red triangle), considering the widespread distribution and various land cover types covering the forest-shrub-grass transitions. These various land types guarantee the generalization of the regression LUT for various vegetation types. The downwelling/upwelling radiation flux measurements rely on solar illumination, and thus, albedo measurements are collected only during the local time of day (mostly from 4 A.M. to 8 P.M.) when sunlight was available. Therefore, we choose suitable albedo samples from all the collected measurements from 4 A.M. to 8 P.M.

The distribution of the observed shortwave broadband albedos and SZAs as a function of local time is shown in Fig. 2(a) and (b), respectively. Outliers of albedo measurements that exceed the physical boundary (0–1) were removed first, and then, a total of 62 859 samples were obtained. The standard deviations are smaller for albedos measured from 8 A.M. to 4 P.M. than the data from the other time period [see Fig. 2(a)], which indicates that daytime measurements are more stable. In addition, the values of SZA and measured albedo are too high before 8 A.M. and after 4 P.M., especially around the sunrise and sunset. The large value of the two parameters may cause much more uncertainties than the relatively smaller variation of albedo values during the daytime. Moreover, SZAs during the daytime from 8 A.M. to 4 P.M. can offer sufficient angle variation [see Fig. 2(b)]. An example is provided to describe the SZA variances at USA site 11 on the 173rd (near summer solstice, hollow triangle) and 355th (near winter solstice, hollow circle) days in 2004 [see Fig. 2(b)], which shows that the SZA changes dramatically over a wide range in summer, while a relatively gentle change for SZAs is observed in winter for SZAs larger than 50°. Around the overpass time of 10:30 A.M. for Landsat in Fig. 2(b) [14], SZA variations cover a wide range from 15° to 75°; this range is sufficient to perform angular bin regression, which usually obtains LUTs for SZAs up to 70° [22], [23], [26], [28]. By comparing Fig. 2(a) and (b), we can see that large albedos (i.e., >0.3) are mainly observed away from local solar noon, especially at large SZAs. In addition, the kernel-driven model is usually not recommended to perform BRDF simulations at

Site No.	Site Name	Network	Country	Latitude (degrees (°))	Longitude (degrees (°))	IGBP Class	Temporal Range	Years for Assessment	Tower Height Above Canopy /footprint (m)
1	AU-Tum	FLUXNET	Australia	-35.66	148.15	EBF	2001-2011	2004, 2005	31.5/398
2	AU-Wac	FLUXNET	Australia	-37.43	145.19	EBF	2005-2008	2006, 2007	15/189
3	CA-Ca1	FLUXNET	Canada	49.87	-125.33	ENF	1997-2010	2004, 2005	45/568
4	CA-NS6	FLUXNET	Canada	55.92	-98.96	OSH	2001-2005	2004, 2005	6/76
5	CA-WP1	FLUXNET	Canada	54.95	-112.47	MF	2003-2009	2004, 2005	6/76
6	DE-Geb	FLUXNET	Germany	51.10	10.91	CRO	2001-2011	2004, 2005	5/63
7	ES-LMa	FLUXNET	Spain	39.94	-5.77	SAV	2004-2011	2005, 2006	/40
8	FR-Hes	FLUXNET	France	48.67	7.07	DBF	1997-2010	2004, 2005	5/63
9	NL-Ca1	FLUXNET	Netherlands	51.97	4.93	GRA	2003-2008	2004, 2005	10/126
10	RU-Che	FLUXNET	Russia	68.61	161.34	MF	2002-2005	2004, 2005	/400
11	US-Aud	AmeriFlux	USA	31.59	-110.51	GRA	2002-2011	2004, 2005	4/51
12	US-Bn1	AmeriFlux	USA	63.92	-145.38	ENF	2002-2004	2003, 2004,	7/88
13	US-Bo1	AmeriFlux	USA	40.01	-88.29	CRO	1996-2008	2004, 2005	10/126
14	US-FPe	AmeriFlux	USA	48.31	-105.10	GRA	2000-2008	2004, 2005	3.5/44
15	US-MMS	AmeriFlux	USA	39.32	-86.41	DBF	1999-2011	2004, 2005	20/253
16	US-SRM	AmeriFlux	USA	31.82	-110.87	WSA	2004-2011	2004, 2005	7.8/99
17	ZA-Kru	FLUXNET	South Africa	-25.02	31.50	SAV	2000-2011	2003, 2007	13/164
18	CA-Ca3	FLUXNET	Canada	49.53	-124.90	ENF	2001-2010		18/227
19	CA-SF2	FLUXNET	Canada	54.25	-105.88	ENF	2002-2005		9/114
20	CA-SF3	FLUXNET	Canada	54.09	-106.01	ENF	2002-2006		20/253
21	CZ-BK1	FLUXNET	Czech Republic	49.50	18.54	ENF	2004-2011		/40
22	DE-Hai	FLUXNET	Germany	51.08	10.45	DBF	2000-2011		10.5/133
23	DE-Kli	FLUXNET	Germany	50.89	13.52	CRO	2004-2011		3.5/44
24	DE-Tha	FLUXNET	Germany	50.96	13.57	ENF	1996-2011		10.5/133
25	DE-Wet	FLUXNET	Germany	50.45	11.46	ENF	2002-2008		10/126
26	FR-Pue	FLUXNET	France	43.74	3.60	EBF	2005-2011		5/63
27	HU-Bug	FLUXNET	Hungary	46.69	19.60	GRA	2002-2008		4/51
28	IE-Dri	FLUXNET	Ireland	51.99	-8.75	GRA	2002-2011		/40
29	IT-Bon	FLUXNET	Italy	39.48	16.54	ENF	2005-2009		/40
30	IT-Col	FLUXNET	Italy	41.85	13.59	DBF	2004-2011		5/63
31	NL-Lan	FLUXNET	Netherlands	51.95	4.90	CRO	2005-2006		/40
32	NL-Loo	FLUXNET	Netherlands	52.17	5.74	ENF	1996-2011		6.39/81
33	PT-Esp	FLUXNET	Portugal	38.64	-8.60	EBF	2004-2008		/40
34	SE-Nor	FLUXNET	Sweden	60.09	17.48	ENF	1996-2008		20/253
35	UK-Gri	FLUXNET	UK	56.61	-3.80	ENF	2000		8/101
36	US-Fmf	AmeriFlux	USA	35.14	-111.73	ENF	2005-2010		/245
37	US-Fuf	AmeriFlux	USA	35.09	-111.76	ENF	2005-2010		23/290
38	US-IB1	AmeriFlux	USA	41.86	-88.22	CRO	2005-2011		4/51
39	US-MOz	AmeriFlux	USA	38.74	-92.20	DBF	2004-2011		30/379
40	US-WCr	AmeriFlux	USA	45.81	-90.08	DBF	1999-2011		122/1541
41	BON	SURFRAD	USA	40.0516	-88.3733	CRO	1995-2011		10/126
42	DRA	SURFRAD	USA	36.6232	-116.0196	OSH	1998-2011		10/126
43	FPK	SURFRAD	USA	48.3080	-105.1018	GRA	1995-2011		10/126
44	GWN	SURFRAD	USA	34.2547	-89.8729	GRA	1995-2011		10/126
45	PSU	SURFRAD	USA	40.7203	-77.9310	CRO	1998-2011		10/126
46	SXF	SURFRAD	USA	43.7343	-96.6233	GRA	2003-2011		10/126
47	TBL	SURFRAD	USA	40.1256	-105.2378	GRA	1995-2011		10/126

The dataset is labelled by IGBP class. Evergreen Needleleaf Forest (ENF, IGBP=1); Evergreen Broadleaf Forest (EBF, IGBP=2); Deciduous Broadleaf Forest (DBF, IGBP=4); Mixed Forest (MF, IGBP=5); Open Shrubland (OSH, IGBP=7); Woody Savanna (WSV, IGBP=8); Savanna (SAV, IGBP=9); Grassland (GRA, IGBP=10); and Cropland (CRO, IGBP=12).

dusk or dawn due to the large SZAs [33], [42]. Consequently, considering the sufficient SZAs and fewer uncertainties in the albedo measurements, only flux records from 8 A.M. to 4 P.M. were selected to build and assess the regression LUT of the direct-estimation algorithm [33].

The measured albedo data set for 15 different SZAs (i.e., 10°, 15°, 20°, . . . , 75°, and 80°) was used to perform the angle bin regression and to obtain the LUT for each SZA according to previous studies [23], [28]; a total of 16 140 samples were eventually collected with SZAs near the 15 values within ±1° [see Fig. 2(c)]. For example, the final regression LUT for SZA = 10° was calculated by using albedos at SZAs of 9°–11°. The larger the SZAs, the greater the variances in albedo. Generally, the data set has a wide range of angle indexes for the anisotropy flat index (AFX) as introduced in Section III-A and NDVI, which was calculated by using
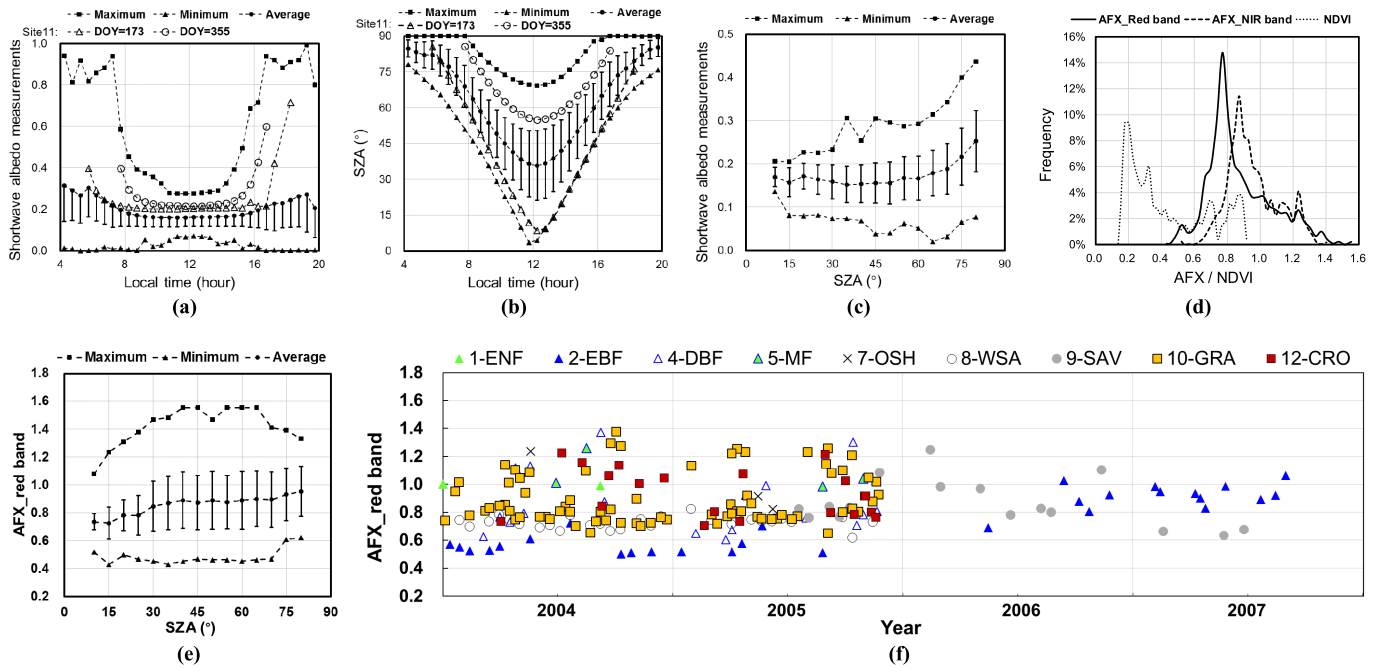
Fig. 2. Data set variations, including albedo, SZA, local time, NDVI, and anisotropy flat index (AFX). (a) Relationship between the local time and albedo. (b) Relationship between the local time and SZA. (c) Relationship between the SZA and albedo. Error bars refer to one standard deviation in (a)–(c). (d) Distributions of AFX and NDVI. (e) Relationship between the SZA and AFX in the red band. (f) Variation in the AFX in the red band for nine IGBP types during 2004–2007.

the MODIS BRDF parameters [see Fig. 2(d)], indicating that a comprehensive consideration has been taken in the data set for variations in both angular and spectral domains. Notably, half of the data set (8070 samples) was randomly selected to build the regression LUT, and the other half were used to assess the LUT to guarantee a completely independent analysis with a similar sampling distribution, as shown in Fig. 2(c) and (d). For each SZA, the training and assessment data set had the same samples, and the number of samples can be seen in Table II. All the large albedos were representative of herbaceous land cover, including savanna (sites 7 and 17), grassland (sites 9, 11, and 14), and cropland (site 13). Measured surface albedos larger than 0.3 mainly occurred for land surfaces without vegetation, such as in winter, and some observed albedos were probably increased by high reflectance caused by buildings near the observation flux tower. Except for bare soil in winter, most of the observed areas were covered with herbaceous vegetation, where a high SZA is mainly responsible for the large albedos. In general, the distribution of large albedos conforms to the SZAs and soil–vegetation land cover variations, and therefore, the albedo training data set can support the generalization of the algorithm.

The snow-free albedo observation data set for 17 sites during two years includes the entire growth season of nine types of vegetation, and thus, the final regression LUT is a generalization of BRDF variations as a function of season, location, and land cover type. The distribution of the AFX [see Fig. 2(d)] shows a wide range of BRDF variations for the entire training data set, and we further analyzed the BRDF variations with changes in the SZA, time, and IGBP type based on the AFX, as shown in Fig. 2(e) and (f) and Table II.

The statistics show that the variations in the AFX in the red band for each SZA are generally quite broad, varying from 0.43 to 1.55. The standard deviation of the AFX changes from 0.06 to 0.21, with an average of 0.17. Seasonally, the AFX values of most vegetation types show large variations, among which the AFX of woody savanna remains nearly constant, with a small standard deviation of 0.04.

In situ albedo measurements at all 47 sites across multiple years were collected to validate the algorithm, as listed in Table I, except measurements that were used to build and assess the LUT mentioned above. Notably, very few outliers were removed before implementing the validation, which is obviously abnormal when examining the albedo variations over multiple years at the 47 sites. Satellite signals (i.e., TM TOA reflectances) for these validation sites, as introduced in Section II-C, were used to estimate the surface shortwave broadband albedos, and the average of the albedo measurements within ±30 min near the Landsat overpass time was used to validate the albedo estimations.

B. MODIS BRDF Parameter and Data Quality

Following the earlier direct-estimation method, TOA reflectances are needed to build the regression LUT for surface albedos, and these TOA reflectances have been generally simulated using MODIS BRDF parameter products [22], [23], [28]. Therefore, the 500-m Collection V006 daily MODIS BRDF model parameters (MCD43A1) with good quality (MCD43A2) [32], [39], [43] (https://urs.earthdata.nasa.gov/) were used to simulate the TOA reflectances in this study, which are concurrent with the flux measurements at the first 17 sites for 2004 and 2005. The MCD43A1 data provide the three

TABLE II
AFX VARIATIONS IN THE RED BAND FOR THE TRAINING DATA SET

		Data Number	Min	Max	mean	std
SZA(°)	10	114	0.52	1.08	0.73	0.06
	15	136	0.43	1.24	0.73	0.12
	20	267	0.50	1.31	0.78	0.11
	25	340	0.47	1.38	0.78	0.14
	30	538	0.45	1.47	0.85	0.18
	35	701	0.43	1.48	0.87	0.19
	40	797	0.45	1.55	0.89	0.20
	45	1111	0.47	1.55	0.87	0.20
	50	1104	0.46	1.47	0.89	0.21
	55	1076	0.46	1.55	0.88	0.19
	60	756	0.45	1.55	0.89	0.21
	65	525	0.46	1.55	0.90	0.20
	70	345	0.47	1.41	0.89	0.20
	75	166	0.61	1.39	0.93	0.19
	80	94	0.62	1.33	0.95	0.18
IGBP	1-ENF	17	0.67	1.33	1.03	0.20
	2-EBF	29	0.50	1.06	0.73	0.20
	4-DBF	17	0.60	1.37	0.85	0.23
	5-MF	7	0.83	1.26	1.01	0.15
	7-OSH	3	0.82	1.24	0.99	0.22
	8-WSA	29	0.62	0.83	0.73	0.04
	9-SAV	16	0.63	1.25	0.86	0.17
	10-GRA	75	0.65	1.38	0.90	0.18
	12-CRO	20	0.70	1.22	0.94	0.17

kernel coefficients of the kernel-driven BRDF model, as (1) in Section III-A, which are retrieved by the 16-day aggregations of multiangle reflectances from the MODIS sensors onboard the Terra (overpass at 10:30 A.M.) and Aqua (overpass at 1:30 P.M.) satellites. Only the BRDF parameters with good quality (full inversion, quality flag of 0/1) for the first seven bands were used. To eliminate snow-covered pixels from these MODIS BRDF parameters, the concurrent daily products of MOD10A1 and MYD10A1 from the Terra and Aqua satellites were further used to select the snow-free and cloud-free data (snow cover flag of 0) in addition to using the MODIS BRDF quality product (i.e., MCD43A2). Then, these high-quality MODIS BRDF parameters were used as prior anisotropic information to simulate the TM TOA reflectances for building and assessing the direct-estimation algorithm LUT.

C. Landsat TM TOA Reflectance

To correct the simulated TOA reflectances and perform the algorithm validation, satellite signals of the 30-m Landsat TM were collected. Due to the long-time coverage (1984–2011) of the TM sensor onboard Landsat 4 and 5, we adopted the TM TOA reflectances. The Collection-1 L1TP digital number (DN) data, following radiometric, geometric, and terrain corrections, were downloaded from the USGS website (https://earthexplorer.usgs.gov/). The time and locations of these TM reflectances are listed in Table I. Pixels with a high-quality flag

of 672 were used, which are indicative of clear days and not affected by the saturation issue according to the Band Quality file (https://Landsat.usgs.gov/collectionqualityband). TOA spectral reflectance data were derived from the DN value based on the conversion coefficients provided in the metadata file [23]. The SZA for each scene was also extracted from the metadata file for algorithm analysis and application.

In total, two data sets of TM TOA reflectances were collected. First, 161 sets of TOA spectral reflectances were used to correct the TOA reflectance simulations for building the regression LUT, which are concurrent with the flux measurements at the first 17 sites in 2004 and 2005. In addition, excluding the data used for LUT correction, 1578 sets of data from all 47 sites in the multiple year cycle, as listed in Table I, were collected to validate the algorithm. Among the validation data, 687 sets of TOA spectral reflectances at the seven SURFRAD sites were obtained. These 1578 sets of TOA reflectances were used to estimate surface shortwave broadband albedos using the regression LUT, and then, the discrepancies between the estimated and measured albedos were investigated.

III. METHODS

In this article, daytime time-series (30 min or 1 h) radiative flux measurements at the first 17 representative sites over two years, which are listed in Table I, were first used to build and assess the regression LUT of the direct-estimation albedo method as shown in the flowchart (see Fig. 3). Surface shortwave broadband albedo measurements were then calculated as the ratio of the upwelling portion to the total downwelling solar radiation, and the corresponding SZAs were extracted based on the measurement time and site geolocations. These albedo measurements were used instead of simulated albedos, which were derived from MODIS BRDF parameters using the kernel-driven model in the original direct-estimation method [23], with the aim to reduce the algorithm uncertainties for albedo simulations.

Daily MODIS BRDF parameters that are concurrent with these flux measurements were used to simulate the TOA spectral reflectance at the TM bands via the direct-estimation method [23]. The BRDF parameters and SZAs were first input into the kernel-driven model to simulate the surface reflectances at the TM bands based on the band conversion coefficients between MODIS and TM [23], and the hotspot-revised version of the BRDF model [i.e., the Ross-Thick-Chen-Li-Sparse-Reciprocal (RTCLSR) model] was used to obtain accurate directional reflectance [44]. Then, the surface reflectances were transferred to TOA reflectances with the 6S atmospheric radiative transfer model by considering seven aerosol optical depths (AODs) for continental aerosol.

The total concurrent data set (16 140 samples), including albedo and SZA measurements as well as TOA reflectance simulations, was randomly divided into two parts (8070 samples for each part): one part was used to build the regression LUT and the other part was to assess the LUT. Thus, the data used to assess the LUT were independent of the data used to build the direct-estimation algorithm LUT.
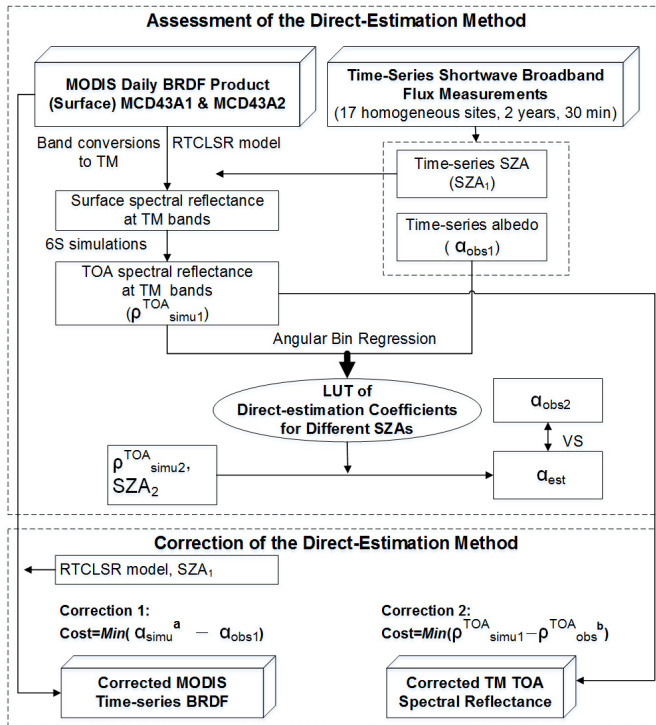
Fig. 3. Assessment and correction flowchart of the direct-estimation surface albedo algorithm for Landsat TM using time-series flux measurements. Half of the entire data set was used to build the regression LUT (SZA$_1$, $\alpha_{\text{obs}1}$, and $\rho_{\text{simu}1}^{\text{TOA}}$), and the other half was used to assess the LUT (SZA$_2$, $\alpha_{\text{obs}2}$, and $\rho_{\text{simu}2}^{\text{TOA}}$). ^{a} Simulated shortwave broadband albedo simulations (α_{simu}) are calculated using the MODIS BRDF parameters and time series of SZA$_1$ using the RTCLSR model. ^{b} Measured TOA reflectances ($\rho_{\text{obs}}^{\text{TOA}}$) refer to the satellite signals (i.e., Landsat TM TOA reflectances), which are concurrent with the half data set in building the LUTs.

By applying concurrent surface albedo measurements and TOA signals (i.e., TOA reflectance) from the Landsat TM as prior knowledge, a two-step correction strategy is proposed to reduce uncertainties caused by BRDF variations and spatial inconsistencies in the TOA reflectance simulation process. This two-step correction method first assumes that the uncertainties in the simulated MODIS albedos based on the MODIS BRDF parameters and the kernel-driven model [33] originate from similar BRDF shapes to varying degrees. Therefore, the magnitude inversion method is used to linearly adjust the BRDF parameters to meet the albedo measurement magnitudes (hereinafter, correction 1). Second, the uncertainties underlying the simulated TOA nadir reflectances that were spectrally transferred to the TM bands may originate from the unresolved scaling problem between the MODIS and TM data and the atmospheric correction process according to previous studies [23], [36]–[38], [45]. To reduce these uncertainties, the Landsat TM signals (i.e., Landsat TM TOA reflectances) concurrent with the flux measurements were directly used to correct the differences (hereinafter, correction 2), although there were fewer TM observations than flux measurements. Notably, this correction is very straightforward for addressing possible scale effect in the near-nadir direction; more efforts are needed to study the scale effect in BRDF variations at different spatial resolutions [36]–[38].

Finally, based on the first part of the entire data set, which was used to build the LUT, two LUTs between TOA spectral reflectance simulations at the TM bands and surface shortwave broadband albedo measurements for different SZAs were built before and after using the two-step correction strategy. Then, the surface albedos were estimated from the second part of the independent TOA reflectance simulations at certain SZAs by using the two LUTs, and these estimations were compared with albedo measurements to assess both LUTs. In addition, TM TOA reflectance observations at 47 sites in a multiyear cycle were also used to validate both LUTs.

In Sections III-A–III-D, we illustrate in detail the methods used to build, improve, assess, and validate the regression LUT.

A. Building the Regression LUT of the Direct-Estimation Method Based on Flux Measurements and Concurrent Daily MODIS BRDF Parameters

The flux measurements at 17 sites over 2 years, as mentioned in Section II-A, were first used to build the regression LUT of the direct-estimation method, and albedos at 15 SZAs (i.e., $10°$, $15°$, $20°$, ..., $75°$, and $80°$) were extracted from the data set. Then, concurrent daily MODIS BRDF parameters were transferred to the result at the TM bands by applying the band conversion coefficients published by He *et al.* [23]. Following the traditional direct-estimation algorithm, the kernel-driven BRDF model was adopted to simulate the surface bidirectional reflectances because of the model's robust BRDF description [4], [5], [44]–[46], and the general expression is given in (1). Here, a hotspot-revised version of the model was used, which is called the RTCLSR model [44]

$$R(\theta_s, \theta_v, \varphi, \lambda) = f_{\text{iso}}(\lambda) + f_{\text{vol}}(\lambda)K_{\text{vol}}(\theta_s, \theta_v, \varphi) \\ + f_{\text{geo}}(\lambda)K_{\text{geo}}(\theta_s, \theta_v, \varphi). \quad (1)$$

In (1), R refers to the surface directional reflectance as a function of three angles [SZA (θ_s), VZA (θ_v), and RAA ($\varphi\varphi$)] and a waveband λ, which is composed of three scattering types, including isotropic scattering (1.0), volumetric scattering (K_{vol}), and geometric-optical scattering (K_{geo}). By inputting multiangle reflectances to the model, the three weight coefficients of f_{iso}, f_{vol}, and f_{geo} can be determined based on the least-squares regression. Subsequently, directional reflectances at arbitrary orientations can be simulated, from which we can obtain the directional hemisphere albedo [black sky albedo (BSA)] and bihemisphere albedo [white sky albedo (WSA)], which are integrals over only the reflected hemisphere or bihemisphere. The angle index AFX is defined as the ratio of the WSA to f_{iso}, which is sensitive to the scattering type [47]. An AFX value larger than 1.0 means that volumetric scattering is prominent, while an AFX value of less than 1.0 indicates dominant geometric scattering.

According to the traditional direct-estimation method, directional reflectances at the land surface must be transferred to the results above the TOA. Here, to avoid extremely large computations, a fast and accurate atmospheric radiative transfer model [48] was used, which can infer atmospheric

process variables from 6S simulations based on the MODIS BRDF parameters and aerosol types. This simplified model has been used in the direct-estimation albedo algorithm for MODIS and VIIRS sensors [26], [28]. Then, TOA reflectance can be calculated by considering these variables, and the model equations are as follows:

$$\rho^{\text{TOA}}(\theta_s, \theta_v, \varphi)$$
$$= \rho_0(\theta_s, \theta_v, \varphi)$$
$$+ \frac{T(\theta_s) R(\theta_s, \theta_v, \varphi) T(\theta_v) - t_{\text{dd}}(\theta_s) t_{\text{dd}}(\theta_v) |R(\theta_s, \theta_v, \varphi)| \overline{\rho}}{1 - r_{\text{hh}} \overline{\rho}}$$
(2)

$$T(\theta_s) = \begin{bmatrix} t_{\text{dd}}(\theta_s) & t_{\text{dh}}(\theta_s) \end{bmatrix}$$
(3)

$$T(\theta_v) = \begin{bmatrix} t_{\text{dd}}(\theta_v) & t_{\text{hd}}(\theta_v) \end{bmatrix}^T$$
(4)

$$R(\theta_s, \theta_v, \varphi) = \begin{bmatrix} r_{\text{dd}}(\theta_s, \theta_v, \varphi) & r_{\text{dh}}(\theta_s) \\ r_{\text{hd}}(\theta_v) & r_{\text{hh}} \end{bmatrix}$$
(5)

where $\rho^{\text{TOA}}(\theta_s, \theta_v, \varphi)$ refers to the TOA reflectance. The four reflectance variables r_{dd}, r_{dh}, r_{hd}, and r_{hh} included in $R(\theta_s, \theta_v, \varphi)$ represent bidirectional, directional-hemispheric, hemispheric-directional, and bihemisphere surface reflectances, respectively, which can be calculated by the kernel-driven model. The remaining six-independent atmospheric radiative transfer variables were simulated using the 6S model, including the downward bidirectional path transmittance $[t_{\text{dd}}(\theta_s)]$, directional-hemispheric path transmittance $[t_{\text{dh}}(\theta_s)]$, upward bidirectional path transmittance $[t_{\text{dd}}(\theta_v)]$, hemispheric-directional path transmittance $[t_{\text{hd}}(\theta_v)]$, atmospheric path reflectance $[\rho_0(\theta_s, \theta_v, \varphi)]$, and spherical albedo of the atmosphere $(\overline{\rho})$. We used the popular "US62" standard atmospheric model, in which water vapor, ozone, and CO_2 settings are prescribed with the change of altitude [30]. The continental aerosol type was set using seven AODs in the 6S simulations, including 0.05, 0.10, 0.15, 0.20, 0.30, 0.40, and 0.60, as designed in previous studies [22], [23]. Subsequently, we obtained the TOA reflectances by (2) with the aid of these four reflectance variables and six radiative transfer variables.

Then, the concurrent surface shortwave broadband albedo measurements and TM TOA spectral reflectance simulations (8070 samples) at 7 AODs (8070 × 7 samples in total) were used to perform the multiple linear regressions to obtain LUTs at 15 SZAs. Thus, the regression LUTs between the TM TOA spectral reflectance and the surface broadband albedos at 15 different SZAs were built.

B. Building the Regression LUT Based on the Proposed Two-Step Correction Strategy

To further improve the method, we investigated the uncertainties underlying the method. As it is known, there remain errors in estimating surface albedos based on the MODIS BRDF parameters within an RMSE of 0.05 [6], [33], [34], [40]. Therefore, we first investigated the MODIS BRDF parameter errors in the albedo simulation. MODIS albedos simulated by the daily MODIS BRDF parameters through the kernel-driven model are not always consistent with albedo
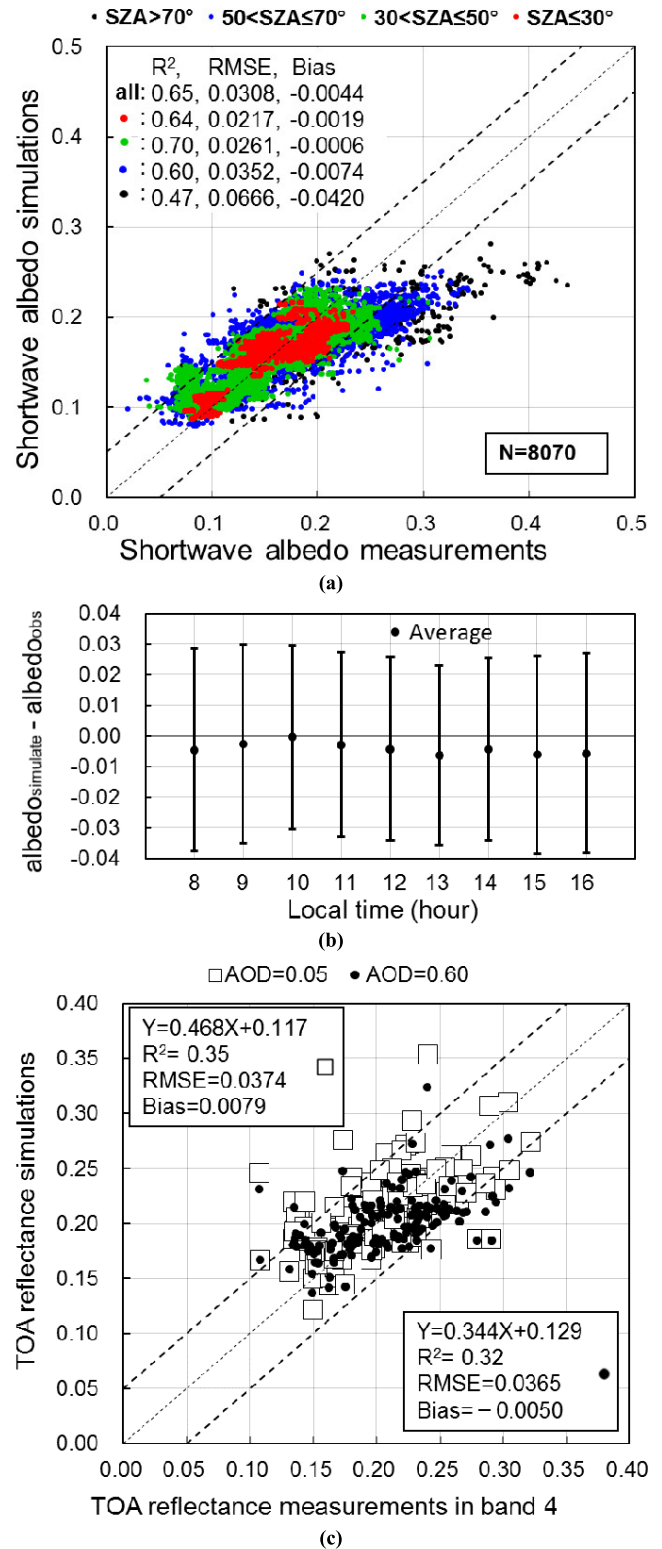

Fig. 4. Uncertainties in the direct-estimation albedo method. (a) Comparison between simulated albedos based on the MODIS BRDF parameters and measured albedos. (b) Average and one standard deviation between the albedo simulations and measurements. (c) Comparison of the TOA reflectances between the simulation results for AODs of 0.05 (square) and 0.60 (dots) and those of the TM observations in the near infrared (i.e., band 4).

measurements, as shown in Fig. 4(a). Generally, underestimations are more obvious as the SZA increases, which is in accordance with the previous validation results [33] and

may be ascribed to the model performance at large SZAs [4], [5]. In addition, the albedo discrepancies vary over time during a day with a standard deviation of 0.03, and the optimal consistencies between the simulated and measured albedos are observed at approximately 10 A.M. and 2 P.M., which are close to the overpass times of the Terra and Aqua satellites [see Fig. 4(b)]. These discrepancies indicate that researchers should be aware of the BRDF variances during the day, and albedos simulated using the MODIS BRDF parameters are inconsistent with the measured albedos.

Considering the albedo measurements, those measurements that are close to the "true values" were utilized to build the regression LUT, and thus, the main method uncertainties will result from the TOA simulation. Consequently, we further checked the accuracy of the final TOA reflectance simulations. In total, 161 sets of TM TOA spectral reflectances, as introduced in Section II-C, were used as the reference data to perform the examination, which are concurrent in time and location with the data set used to build the method. For example, the linear fitting formulas between the 161 sets of TOA reflectance observations and the simulations obtained from the 6S model and surface BRDF parameters in the near-infrared band are shown in Fig. 4(c). We can see that the slope decreases when the AOD value increases from 0.05 to 0.60, which indicates a larger deviation at large AODs. The slope and offset coefficients in these formulas at all bands are listed in Table II, where the slopes decrease gradually as the AOD increases, providing more detailed evidence. The errors between the simulated TOA reflectances and observations may arise from the BRDF variations from the 500-m MODIS to the 30-m Landsat data.

To reduce the uncertainties caused by data inconsistencies between the MODIS BRDF parameters and observed albedos and the BRDF scale differences between the MODIS and Landsat data during TOA reflectance simulation, a two-step correction strategy is proposed to improve the LUT regression. Albedo measurements and TM TOA reflectances that are concurrent with the LUT data set were introduced into the corrections, and the detailed correction methods are illustrated as follows.

1) Correction of MODIS BRDF Parameters Based on Albedo Measurements Using a Magnitude Method (Correction 1): In the backup algorithm of the operational MODIS BRDF parameter product, a magnitude inversion is performed by assuming that the BRDF shape for a certain land cover is broadly similar [6], [49], and a multiplicative factor is used to adjust the three BRDF parameters to find the optimal multiangle reflectance fitting. Similarly, we assume that each flux site shares a similar BRDF shape that changes with different reflectance anisotropy degrees at a certain time of day, and the albedo uncertainties can be explained as anisotropy degree variations. Therefore, to correct the BRDF, especially at large SZAs, we performed the first step of the correction strategy to linearly adjust the daily MODIS BRDF parameters using the magnitude method to match the albedo time series measurements (every 30 min) (correction 1).

The cost function is shown as (6), where *adjust* refers to the newly introduced adjustment coefficient of the MODIS
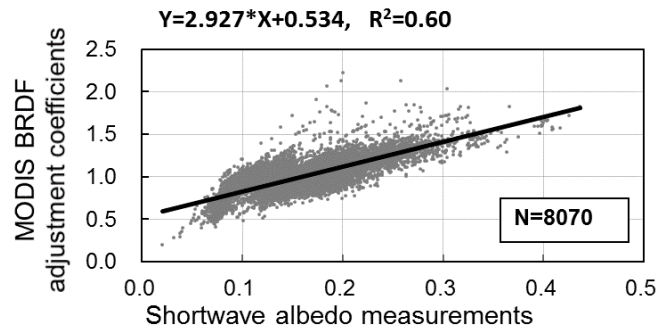

Fig. 5.   Relationship between the MODIS BRDF adjustment coefficients and the measured albedos.

BRDF parameters and is invariable for the three kernel parameters and the first seven bands of the MODIS sensor. In (6), $\text{sw\_albedo}_{\text{obs}}$ represents the shortwave broadband albedo measurements, and $\text{sw\_albedo}_{\text{simulate}}$ represents the albedos simulated by the kernel-driven model with a general percentage of diffuse skylight (i.e., 20%) due to the lack of measurements from tower albedometers [23]. The narrowband-to-broadband conversion coefficient $\text{coe}(\lambda)$ for MODIS was referenced in the results of Liang's study [50]. Based on (6), we aim to find the proximal adjustment coefficients of the MODIS BRDF parameters to guarantee the closest albedo simulations retrieved by the kernel-driven model to the actual albedo measurements

$$
\begin{aligned}
\text{Cost} = \text{MIN} \Bigg(& \text{adjust} * \text{sw\_albedo}_{\text{simulate}} \\
& \times \left(\sum_{\lambda=1}^{7} \text{coe}(\lambda)(0.8 * \text{BSA}(\theta_s, \lambda) + 0.2 * \text{WSA}(\lambda)) \right) \\
& - \text{sw\_albedo}_{\text{obs}} \Bigg).
\end{aligned} \tag{6}
$$

The MODIS BRDF parameter adjustment coefficients during a day (see Fig. 5) are equal to the ratio of the albedo measurements to albedo simulations retrieved from the MODIS BRDF parameters based on the kernel-driven model, where the SZA affects the BSA as well as the final ratio. Most of the coefficients are close to unity, ranging from 0.5 to 1.5, which indicates that the BRDF changes within ±50% for varying SZAs from 8 A.M. to 4 P.M. All 8070 sets of MODIS BRDF parameters were adjusted based on specific albedo measurements; then, these corrected BRDF parameters were used for TOA simulations following the general process introduced in Section III-A.

2) Correction of TOA Reflectance Simulations Based on Reflectance Observations (Correction 2): To further reduce the uncertainties caused by BRDF differences between the 500-m MODIS and 30-m Landsat data in the context of TOA simulations, a second correction step was proposed to make the final TOA reflectance simulations more consistent with the observations (correction 2). The adjustment relies on the linear fitting relationships between the 161 sets of TOA reflectance

TABLE III

SLOPE AND OFFSET IN THE LINEAR RELATIONSHIPS BETWEEN THE OBSERVED TOA REFLECTANCES (X) AND SIMULATED REFLECTANCES (Y) FOR CORRECTION 2

		Slope						Offset					
	AOD\Band	1	2	3	4	5	7	1	2	3	4	5	7
Before Correction 1	0.05	0.840	0.875	0.900	0.468	0.866	0.835	0.019	0.013	0.011	0.117	0.035	0.021
	0.10	0.810	0.840	0.872	0.455	0.857	0.829	0.026	0.018	0.015	0.118	0.035	0.021
	0.15	0.780	0.805	0.844	0.443	0.849	0.823	0.032	0.024	0.020	0.119	0.036	0.021
	0.20	0.751	0.772	0.816	0.431	0.840	0.817	0.038	0.030	0.024	0.120	0.036	0.022
	0.30	0.696	0.709	0.763	0.408	0.823	0.805	0.051	0.041	0.032	0.123	0.037	0.022
	0.40	0.644	0.651	0.714	0.385	0.806	0.793	0.063	0.051	0.040	0.125	0.037	0.023
	0.60	0.550	0.546	0.622	0.344	0.772	0.771	0.087	0.072	0.057	0.129	0.039	0.024
After Correction 1	0.05	**0.854**	**0.896**	**0.939**	**0.557**	**0.940**	**0.873**	0.019	0.013	0.011	**0.104**	**0.028**	0.021
	0.10	**0.823**	**0.861**	**0.910**	**0.545**	**0.930**	**0.867**	0.026	0.019	0.015	**0.105**	**0.028**	0.022
	0.15	**0.793**	**0.827**	**0.882**	**0.532**	**0.921**	**0.861**	0.032	0.024	**0.019**	**0.106**	**0.028**	0.022
	0.20	**0.763**	**0.794**	**0.854**	**0.519**	**0.912**	**0.854**	0.039	0.030	**0.023**	**0.107**	**0.029**	0.022
	0.30	**0.707**	**0.731**	**0.800**	**0.495**	**0.893**	**0.843**	0.051	0.041	0.032	**0.110**	**0.030**	0.023
	0.40	**0.654**	**0.673**	**0.749**	**0.471**	**0.875**	**0.831**	0.064	0.051	0.040	**0.112**	**0.030**	0.023
	0.60	**0.559**	**0.567**	**0.656**	**0.426**	**0.839**	**0.807**	0.087	0.072	**0.056**	**0.117**	**0.032**	0.024

The relationship form is shown as "$Y = slope \times X + offset$". The spectral ranges at the six bands of Landsat TM are 0.45-0.52, 0.52-0.60, 0.63-0.69, 0.76-0.90, 1.55-1.75, and 2.08-2.35 μm.

observations and the simulations obtained from surface BRDF parameters, such as the results shown in Fig. 4(c).

The coefficients (slope and offset) in these linear relationships before and after using correction 1 are shown in Table III, and the values highlighted in bold indicate that the TOA reflectance simulations are more consistent with reflectance observations after using correction 1 than the results before using correction 1 (or vice versa). All the slopes in the relations after using correction 1 become larger than the results before using correction 1, which indicates that correction 1 is very helpful for obtaining accurate BRDF information for a specific time during a day. In addition, most of the offsets in the relations are similar before and after using correction 1 except in bands 4 and 5, which have smaller deviations after using correction 1. As the AOD increases, the slopes become larger, which shows greater discrepancies in the TOA reflectance simulations than in the observations. In addition, the consistency between the simulated TOA reflectances and the observed reflectances changes with spectral bands, where the results at red band 3 show high consistency, and large errors occur at near-infrared band 4. Users can refer to these coefficients when undertaking related studies or calculating specific results for other areas and periods.

The coefficients that are extracted from limited data after using correction 1 for different AODs and bands were further applied to adjust the 8070 sets of TOA spectral reflectance simulations. Thus, the two-step correction strategy was completed. The new regression LUTs can be built based on surface albedo measurements and corrected TOA reflectance simulations, where the albedo measurements are from the same data set as that used in Section III-A.

C. Assessment of the Regression LUTs Before and After Using the Correction Strategy

The independent data set of TOA reflectance simulations at 7 AODs and 15 SZAs as well as surface albedo measurements was used to assess the regression LUTs before and after using

such a correction strategy. Surface albedos were estimated from these TOA reflectance simulations using the two LUTs, and then, these estimated albedos were compared with the measured albedos. In particular, we analyzed the accuracies of the two LUTs in the albedo estimation with SZA changes.

D. Validation of the Algorithm Using TM TOA Reflectances and Flux Measurements

Flux measurements and TM TOA reflectances at 47 sites for multiple years and clear days were used to validate the two kinds of regression LUTs before and after using the two-step correction strategy, where albedo estimations retrieved from TOA reflectances using these regression LUTs were compared to ground measurements. We first analyzed the accuracy and time continuity of albedo estimation using flux measurements at the SURFRAD network sites. Then, a data set from sites 1–40 and four homogeneous SURFRAD network sites were used for the overall validation. The albedo estimation accuracies with SZA changes were also investigated.

IV. RESULTS AND ANALYSIS

A. Assessment Results Based on Daytime Time-Series Flux Measurements and TOA Reflectance Simulations

The comparison between estimations and measurements of shortwave broadband albedo is shown in Fig. 6, where the albedo estimations were completely calculated from independent TOA reflectance simulations (8070 samples) as introduced in Section II-A based on the regression LUTs before and after using the two-step correction strategy. In a previous study based on the albedo simulations of He *et al.* [23], the algorithm shows that the RMSEs between the estimated albedos and the simulated albedos are less than 0.03 when the SZAs are not larger than 70°. However, based on albedo measurements using the LUT before using the correction strategy in this study, the RMSEs between the estimated albedos and the measured albedos are larger than 0.03 when the SZA exceeds 60°
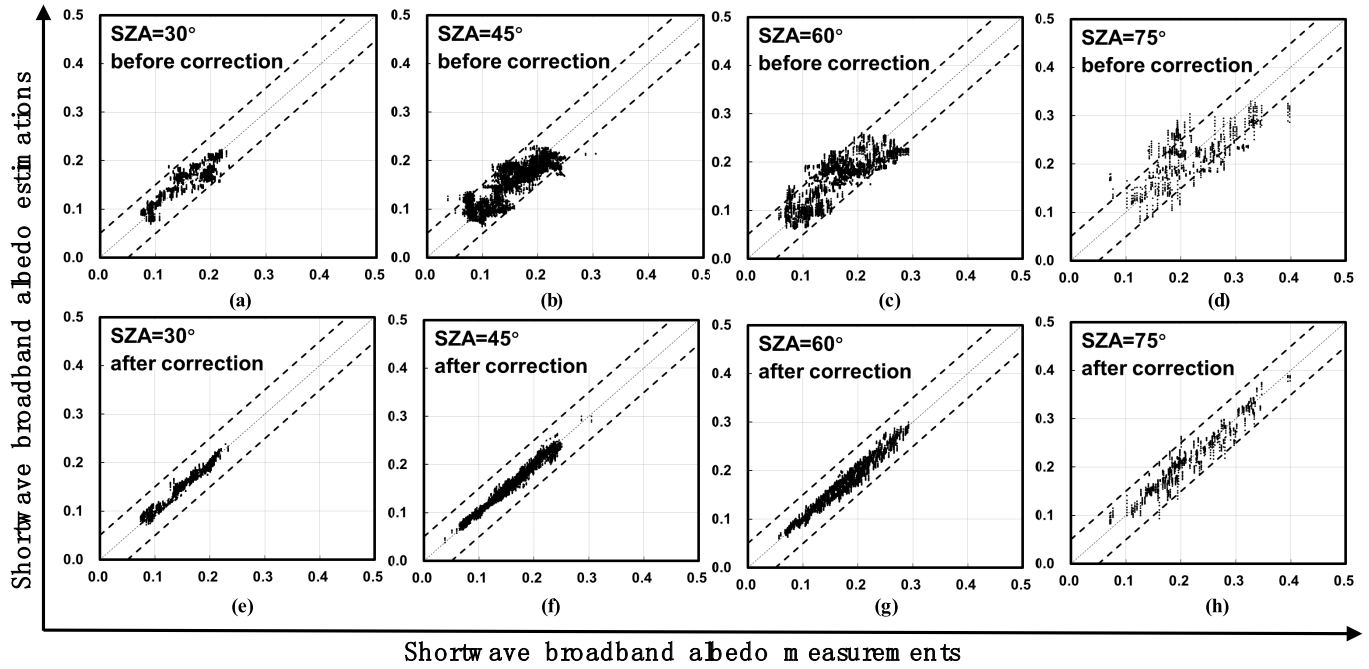
Fig. 6. Comparison of albedo estimations retrieved from TOA reflectance simulations using regression LUTs against albedo measurements. (a)–(d) Results based on the LUT (before correction) for the SZAs of 30°, 45°, 60°, and 75°, respectively. (e)–(h) Results based on the improved LUT (after corrections 1 and 2) at the four typical SZAs similar to (a)–(d).

TABLE IV
ACCURACY OF SURFACE ALBEDO ESTIMATION FROM THE SIMULATED LANDSAT TM TOA REFLECTANCES

Number	SZA (degrees (°))	RMSE			R^2		
		Before Correction	After Correction 1	After Corrections 1+2	Before Correction	After Correction 1	After Corrections 1+2
795	10	0.0082	0.0037	0.0033	0.87	0.97	0.98
952	15	0.0125	0.0053	0.0053	0.86	0.97	0.97
1872	20	0.0150	0.0056	0.0057	0.75	0.97	0.96
2377	25	0.0174	0.0065	0.0061	0.74	0.96	0.97
3766	30	0.0197	0.0075	0.0071	0.76	0.97	0.97
4907	35	0.0202	0.0080	0.0076	0.77	0.96	0.97
5582	40	0.0223	0.0082	0.0073	0.74	0.97	0.97
7774	45	0.0256	0.0082	0.0069	0.69	0.97	0.98
7731	50	0.0281	0.0087	0.0076	0.67	0.97	0.98
7532	55	0.0290	0.0092	0.0086	0.67	0.97	0.97
5292	60	0.0310	0.0108	0.0102	0.63	0.96	0.96
3672	65	0.0330	0.0118	0.0112	0.60	0.95	0.95
2415	70	0.0372	0.0155	0.0148	0.59	0.93	0.94
1162	75	0.0465	0.0190	0.0183	0.50	0.92	0.92
661	80	0.0548	0.0256	0.0253	0.41	0.87	0.87

Number indicates the total number of samples at each SZA for the seven AODs.

[see Fig. 6(a)–(d) and Table IV]. Apparently, the assessment based on albedo measurements in this study shows more uncertainties in the direct-estimation method than He's study. Radiometric uncertainty in either MODIS or Landsat TM data in the training data set may cause errors. Overall, the new assessment results based on the measured albedos are more reliable than those of He's study fully based on the simulated albedos.

A better agreement between albedo estimations and albedo measurements for each SZA is shown for the regression LUT after using the two-step correction strategy introduced in Section III-B [see Fig. 6(e)–(h)] than for that before using the two-step correction strategy [see Fig. 6(a)–(d)]. From Table IV, the RMSEs show a significant decrease after using correction 1, and then, the RMSEs are reduced by 0.0049–0.0295 for the improved LUT (after corrections 1 and 2) compared
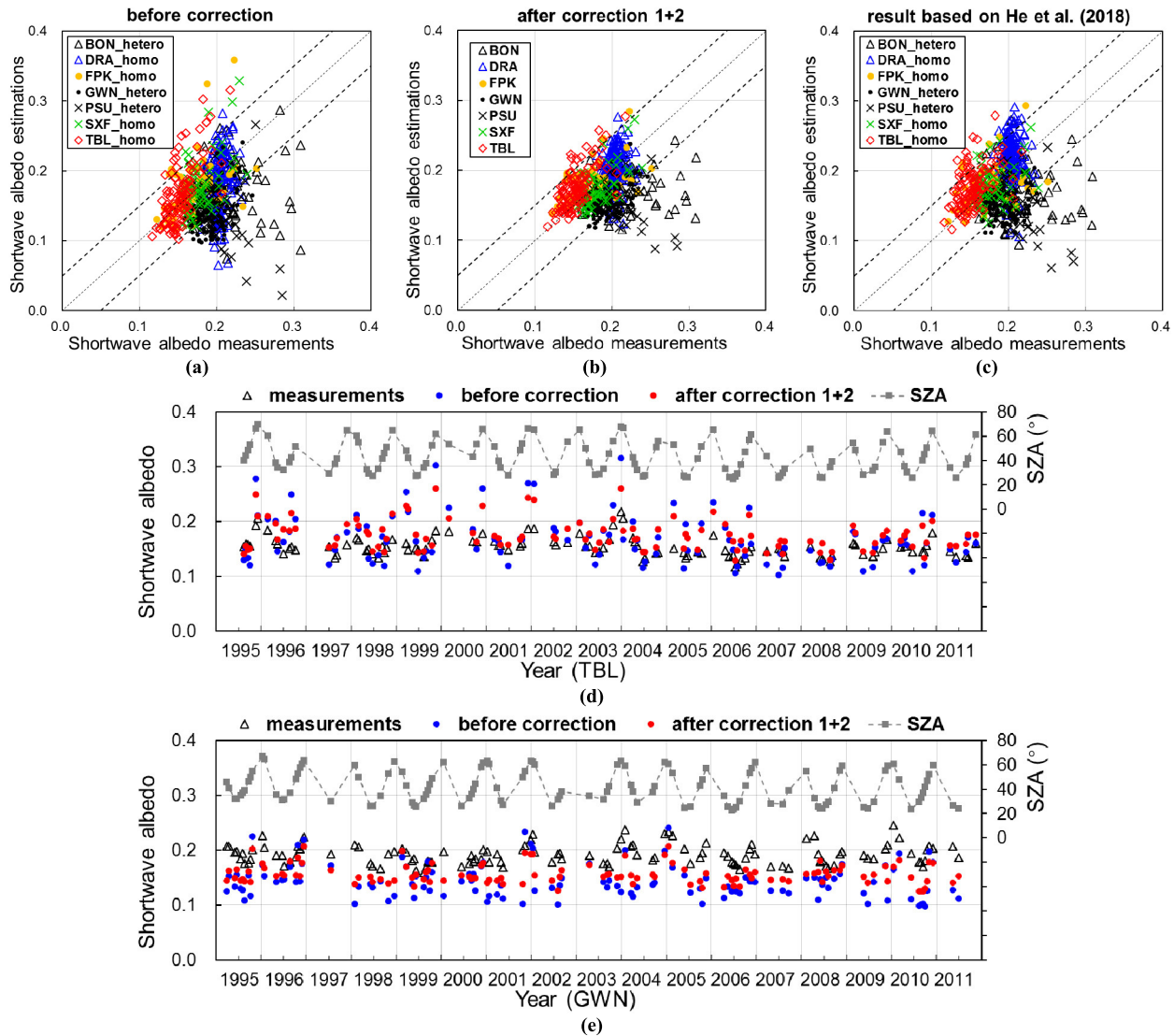
Fig. 7. Comparison between the albedo estimations based on the direct-estimation method and albedo measurements at sites in the SURFRAD network. (a) Results based on the precorrection LUT. (b) Results based on the LUT after the two-step correction strategy. (c) Results based on He *et al.* [23]. (d) Temporal continuity at the homogeneous TBL site. (e) Temporal continuity at the heterogeneous GWN site.

with the original LUT (before correction) when the SZA changes from 10° to 80°. Particularly, the improvements are more prominent at large SZAs (i.e., >60°), and the RMSE is reduced from 0.0548 to 0.0253 when the SZA reaches 80°. The LUT (after correction) presents a high accuracy, with RMSEs of less than 0.02 at SZAs ≤ 75°. In addition, the determination coefficient R^2 is larger than 0.87 for all SZAs and gradually increases from "before correction" to "after correction 1" and then to "after corrections 1 and 2," and the total accuracy is higher than the results in Fig. 2(c) and (d) of He's study [23]. When the SZA reaches 70°, a total RMSE of 0.025–0.030 in estimating the BSA and WSA is observed for He's approach, and the two-step correction strategy shows a significant improvement in the albedo estimations (RMSE = 0.0148). Therefore, compared with the results calculated from the fully simulated data set used in He's study, the observed albedo and simulated TOA reflectances after applying the corrections procedures show better consistency. The basic notion that errors

increase as SZA increases remains true, which is consistent with previous studies on the direct-estimation albedo method [22]–[24], [26], [28]. These improvements show the potential of the two-step correction strategy in estimating albedos with a higher accuracy than He's approach.

B. Validation Results Based on In Situ Measurements

The validation results for both LUT types before and after using the two-step correction strategy proposed in Section III-B for the seven SURFRAD sites (687 samples) are shown in Fig. 7(a) and (b), and the results based on He *et al.* [23] are shown in Fig. 7(c). Clearly, albedos show an underestimation at the three heterogeneous sites of BON, PSU, and GWN, which confirms the findings of earlier studies [14], [34]. Complying with the assessment result of the method in Section IV-A, the validation results also show better consistency between albedo estimations and albedo

TABLE V
ACCURACY OF THE DIRECT-ESTIMATION METHOD BASED ON THE VALIDATION RESULTS

Site	Number	Correction	RMSE	Bias	R^2	Bias> 0.05 (%)	Bias <-0.05 (%)	|Bias| >0.05 (%)
41~47 (SURFRAD)	687	before	0.0526	-0.0226	0.03	4.66	23.73	28.38
		after 1	0.0474	-0.0132	0.02	5.97	17.47	23.44
		after 1+2	0.0379	-0.0118	0.07	2.04	12.81	14.85
		He et al. (2018)	0.0449	-0.0085	0.02	7.28	16.45	23.73
42,43,46,47 (Homogeneous)	424	before	0.0406	-0.0059	0.14	7.08	11.08	18.16
		after 1	0.0329	0.0070	0.28	8.96	4.01	12.97
		after 1+2	0.0254	0.0065	0.38	3.30	1.89	5.19
		He et al. (2018)	0.0329	0.0126	0.31	11.08	3.07	14.15
1-40, 42,43,46,47 All SZAs	1315	before	0.0442	-0.0047	0.32	9.43	13.38	22.81
		after 1	0.0418	0.0045	0.34	10.27	9.51	19.77
		after 1+2	0.0383	0.0107	0.38	11.25	5.10	16.35
		He et al. (2018)	0.0418	0.0110	0.34	13.08	6.54	19.62
1-40, 42,43,46,47; SZA≤30°	270	before	0.0431	-0.0195	0.20	4.07	21.85	25.93
		after 1	0.0347	0.0062	0.37	9.26	8.52	17.78
		after 1+2	0.0308	0.0028	0.43	5.56	4.81	10.37
		He et al. (2018)	0.0379	0.0194	0.43	17.04	1.85	18.89
1-40, 42,43,46,47; 30<SZA≤50°	676	before	0.0386	0.0019	0.39	10.06	7.69	17.75
		after 1	0.0408	0.0093	0.35	11.69	6.07	17.75
		after 1+2	0.0379	0.0153	0.39	12.72	3.11	15.83
		He et al. (2018)	0.0404	0.0142	0.37	13.61	4.29	17.90
1-40, 42,43,46,47; 50<SZA≤70°	362	before	0.0542	-0.0062	0.32	12.15	17.96	30.11
		after 1	0.0486	-0.0056	0.31	8.56	16.85	25.41
		after 1+2	0.0440	0.0077	0.35	12.71	9.12	21.82
		He et al. (2018)	0.0472	-0.0015	0.29	9.12	14.36	23.48
1-40, 42,43,46,47; SZA>70°	7	before	0.0393	0.0113	0.62	14.29	0.00	14.29
		after 1	0.0266	-0.0011	0.79	0.00	0.00	0.00
		after 1+2	0.0435	0.0278	0.92	14.29	0.00	14.29
		He et al. (2018)	0.0608	0.0259	0.35	14.29	0.00	14.29

measurements for the LUT after using the two-step correction strategy proposed in this article.

We further examined the temporal continuity of the method at two sites from 1995 to 2011, as shown in Fig. 7(d) and (e). There is good agreement between the estimated albedos and the measured albedos for the homogeneous TBL site, where large discrepancies usually occur at large SZAs that are gathered in winter. In contrast, underestimations can easily be seen for most periods at the heterogeneous GWN site. The common point for the two typical sites is that the albedo estimations for the postcorrection LUT are more consistent (red dots) with the albedo measurements (black dots) than those for the pre-correction LUT (blue dots).

In general, albedo estimations based on the postcorrection LUT show fewer discrepancies with albedo measurements than the results before correction at the SURFRAD sites, as listed in Table V, where the errors decrease gradually from "before correction" to "after correction 1" and then to "after corrections 1 and 2." The percentage of biases between the estimated albedos and the measured albedos exceeding 0.05 is reduced by half from 28.38% (before correction) to 14.85% (after the two-step correction) at the seven sites, and the overall results for the LUT after correction are also shown (RMSE = 0.0379, bias = -0.0118, and R^2 = 0.07). In addition, the results from the four homogeneous sites (424 samples) show a better agreement between the estimated albedos using the postcorrection LUT and the measured

albedos (RMSE = 0.0254, bias = 0.0065, and R^2 = 0.38) than the results at the seven sites (687 samples), and the percentage of albedo estimations with biases exceeding 0.05 decreases from 18.16% to 5.19%. For the LUT without correction, the bias for the 424 sets of homogeneous data (bias = -0.0059) is smaller than that of He's approach (bias = 0.0126). After using the two-step correction strategy, the RMSEs fall from 0.0329 to 0.0254 for He's LUT (reduced by 22.80%), and the percentage of biases exceeding 0.05 drops from 14.15% to 5.19% (reduced by 63.32%). The RMSEs decrease from 0.0406 (before correction) to 0.0254 (after two-step correction) at the four homogeneous sites, which also demonstrates the robustness of the corrected LUT. These improvements indicate that the two-step correction strategy proposed in this study can practically improve the albedo estimation accuracy of albedo estimations.

Considering the heterogeneity of sites [14], three sites in the SURFRAD network were excluded in the final overall validation (BON, GWN, and PSU). In total, 1315 sets of data were collected for validation, including data at sites 1–40 and four homogeneous sites in the SURFRAD network. The comparison of estimated albedo with the measured albedo is shown in Fig. 8, and Table V shows the corresponding accuracies in the albedo estimations. For the LUT without correction, the bias for the complete data set of 1315 samples (bias = -0.0047) is smaller than that of He's approach (bias = 0.0110). Notably, errors in the albedo estimations
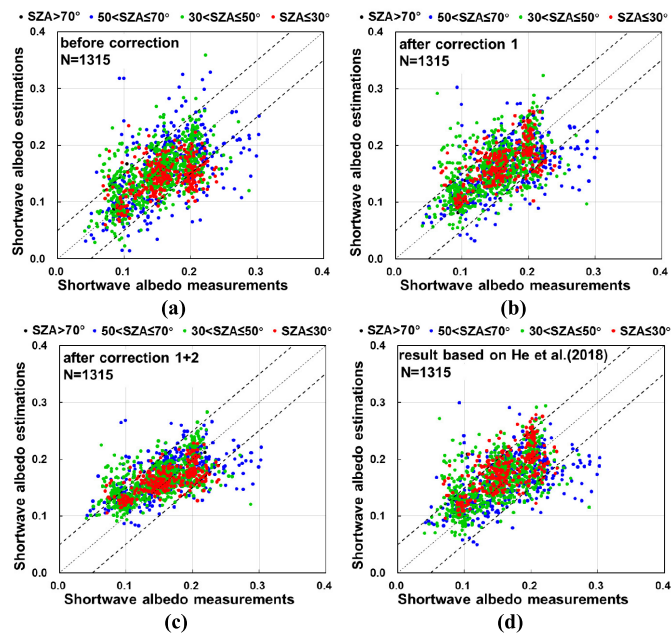
Fig. 8. Comparison between the albedo estimations based on the direct-estimation method and the albedo measurements with SZAs increasing at all 44 sites. (a) Results for the precorrection LUT. (b) Results based on the LUT after correction 1. (c) Results based on the LUT after the two-step correction strategy. (d) Results based on He *et al.* [23].

at SZAs larger than 70° (RMSE = 0.0393, bias = 0.0113, and $R^2 = 0.62$) decrease significantly compared with the results of He's method (RMSE = 0.0608, bias = 0.0259, and $R^2 = 0.35$). This improvement demonstrates the good consistency between the station-measured albedos and the simulated TOA reflectances in training the regression LUT.

Similar to the results at the SURFRAD sites shown in Fig. 7, the LUT after using the first correction further improves the albedo estimation accuracy, especially at SZA exceeding 70° (RMSE = 0.0266, bias = −0.0011, and $R^2 = 0.79$), compared with the estimation results of He's LUT. The second step of the correction strategy further reduces the estimation errors, and the albedo estimations accuracies for all SZAs are also higher at the regression LUT after using the two-step correction strategy (RMSE = 0.0383, bias = 0.0107, and $R^2 = 0.38$) than those before correction (RMSE = 0.0442, bias = −0.0047, and $R^2 = 0.32$). The 22.81% of estimated albedos (before correction) are the so-called outliers with biases exceeding 0.05, while the percentage was reduced to 16.35% when the postcorrection LUT was used for the estimation. As the SZA increases, larger discrepancies in albedo estimations can be found. The RMSE increases gradually from 0.0308 to 0.0440 for the first three increasing SZA intervals, which is in accordance with the assessment results in Fig. 2(c) and (d) of He's study [23], Fig. 6, and Table IV. The results for the data at SZAs larger than 70° show large errors, while the insufficient number reduces reliability. In addition, this phenomenon follows the validation results of the MODIS BRDF/albedo product in Fig. 4(a) and Liu's study [33], which indicates that the accuracy of the direct-estimation method inherits the characteristic of the original MODIS BRDF data. Uncertainties caused by measurements at

large SZAs in the training data set may also affect the results. There are relatively fewer SZA measurements at SZAs of less than 20° and larger than 70° in the training data set, as shown in Table II, and thus, these SZA ranges may have a relatively low confidence relative to the other SZA ranges in terms of the data sampling representativeness.

The validation results based on the LUT after using the two-step correction strategy and He's LUT are further compared. For the complete data set of 1315 samples, the RMSE of the albedo estimation for the postcorrection LUT decreases from 0.0418 to 0.0383 calculated by He's LUT (reduced by 8.37%), and the percentage of biases exceeding 0.05 decreases from 19.62% to 16.35% (reduced by 16.67%). For the results at SZAs larger than 70° for the complete data set, the RMSE declines from 0.0608 to 0.0435 (reduced by 28.45%). According to these improvements, the station-measured albedos as well as the two-step correction strategy used in this study help build a more accurate regression LUT than He's LUT, which indicates that there is better consistency between the station-measured surface albedos and the simulated TOA reflectances in this study than the fully simulated training data set of previous study [23]. Overall, the station-measured albedos as well as the two-step correction strategy present an excellent potential to overcome spatial differences. The validation accuracy when applying the two-step corrections is higher than the results of previous work [23], and the RMSEs of the 1315 sets of albedo estimations over snow-free areas decrease from 0.0418 to 0.0383 (reduced by 8.37%). Notably, there is a significant improvement in the albedo estimation at SZA exceeding 70°. In addition, the results at the four homogeneous sites in the SURFRAD network have a higher accuracy for the newly proposed postcorrection LUT (i.e., RMSE = 0.0254). The validation results in this article have made use of all Landsat TM pixels free of cloud contamination and have not considered whether other pixels in the whole image are contaminated. Therefore, the method proposed in this article can be conveniently used to estimate surface albedos as long as the pixel is cloud-free, which guarantees more effective albedo estimations from limited Landsat images that are frequently affected by clouds.

The RMSEs of the estimated albedos based on the two-step correction strategy as a function of season and land cover are shown in Table VI. Results with RMSE > 0.05 are labeled in bold. Most land cover types in winter have RMSEs exceeding 0.05, and the largest total RMSE is largest in winter. Particularly, the accuracy of the albedo estimation is always low for ENF.

Nevertheless, among the 47 reference sites, 44 are distributed over the Northern Hemisphere, and only 3 sites are located in the Southern Hemisphere. Subsequently, some regions have rarely been covered in the data selection, such as tropical forested regions near the equator. Therefore, the accuracy of the new proposed method in these regions needs to be investigated. In addition, considering that the kernel-driven Ross–Li model was originally developed from vegetation canopies and has been widely used for vegetation–soil systems, a new snow kernel that can better model the anisotropic reflectance of pure snow in the kernel-driven BRDF model

TABLE VI

DISTRIBUTION OF THE TOTAL RMSEs BETWEEN 1315 ESTIMATED ALBEDOS (AFTER THE TWO-STEP CORRECTION) AND MEASURED ALBEDOS FOR DIFFERENT SEASONS AND LAND COVER TYPES

Season /IGBP	Spring	Summer	Autumn	Winter	Total
1-ENF	**0.0647**	**0.0588**	0.0459	**0.0532**	**0.0545**
2-EBF	0.0328	0.0380	**0.0539**	0.0291	0.0356
4-DBF	**0.0535**	0.0302	0.0357		0.0391
5-MF		0.0223	0.0229	**0.0614**	0.0213
7-OSH	0.0225	0.0217	0.0268	0.0331	0.0244
8-WSA	0.0327	0.0307	0.0409	**0.0535**	0.0360
9-SAV	0.0204	0.0239	0.0360	0.0251	0.0227
10-GRA	0.0340	0.0230	0.0424	**0.0585**	0.0363
12-CRO	0.0384	0.0485	0.0397	0.0279	0.0402
Total	0.0391	0.0350	0.0396	0.0434	0.0383

framework has been developed [51], [52], which is expected to improve the direct-estimation albedo algorithm for snow areas. Although the US62 atmospheric model used for training data set is reliable in most cases [30], the accuracy of the LUT may be further improved if more accurate values of water vapor can be collected. For example, some other suitable atmospheric type or measurements of atmospheric profile according to the spatial and temporal ranges of the training data set can be used.

V. CONCLUSION

Coarse-resolution BRDF information is widely used as prior knowledge for high-resolution applications. In the direct-estimation albedo algorithm of 30-m Landsat, simulated albedos from 500-m MODIS BRDF parameters are used to build and assess the regression LUT. In this article, time-series (30 min or 1 h) albedo measurements with sufficient SZAs at 17 homogeneous sites worldwide over a two-year period are first introduced. These measurements are used to build the LUT for the nadir view Landsat TM in conjunction with concurrent daily MODIS BRDF parameters to simulate TOA spectral reflectances at the TM bands. Half of the data were randomly selected to build the LUT, and the other half of the data were used to perform the independent accuracy assessment of the LUT by comparing the estimated albedos from TOA reflectance simulations to measured albedos. In addition, based on concurrent albedo measurements and satellite signals (i.e., TM TOA reflectance), we proposed a two-step correction strategy to further reduce uncertainties caused by inconsistencies between the MODIS BRDF parameters and the observed albedos and possible scale issues when applying the MODIS BRDF to Landsat data. Finally, TM TOA reflectance observations at 47 sites in a multiple year cycle were utilized to compare and validate the two LUTs before and after using such a correction strategy. Several findings of this study are reported as follows.

1) These optimized albedo measurements can likely reduce derived uncertainties by using simulated albedos when building the LUT, which was used for albedo estimations in a previous study [23].

2) We assessed the regression LUT using independent flux measurements and investigated the underlying reasons for the uncertainties. The independent assessment shows that estimated albedo errors from TOA simulations using the LUT before correction against measured albedos mainly occur at large SZAs (RMSE > 0.03 at SZAs $\geq$ 60°). In addition, inconsistencies between the MODIS BRDF data and albedo measurements as well as the BRDF variations at different spatial resolutions between MODIS and TM are most likely responsible for these discrepancies.

3) Accordingly, we proposed a two-step correction strategy to correct the two error sources. The magnitude method was first used to linearly adjust the MODIS BRDF parameters to match the flux measurements by assuming that BRDF shapes are similar at the same sites during a given day. Then, satellite signals (i.e., TM TOA reflectances) were used to correct the final TOA reflectance simulations under the assumption that BRDF variation is mainly caused by the difference in spatial resolutions between MODIS and TM. The corrected LUT presents an improved estimation, and the RMSEs are reduced by 0.0049–0.0295 for SZAs 10°–80° (RMSEs < 0.02 at SZAs $\leq$ 75°), particularly in the case of large SZAs (i.e., >60°), where the improvements appear to be the most prominent. In addition, the total accuracy of the postcorrection LUT is higher than the results of He's study [23].

4) The validation results generally comply with the assessment results, demonstrating that the LUT after using such a correction strategy performs well. Among the seven sites in the SURFRAD network, the four homogeneous sites show more robust estimations than the other three heterogeneous sites, and the RMSEs are 0.0406 and 0.0254 for the LUTs before and after the two-step correction strategy at the four homogeneous sites, respectively. For all 44 homogeneous sites in the multiyear cycle (1315 samples), the RMSE increases as the SZA increases and is reduced to 0.0383 (after the two-step correction strategy) from 0.0442 (before correction) for all SZAs. The percentage for the so-called outliers with biases between estimations and measurements exceeding 0.05 decreases from 22.81% to 16.35%.

5) Compared to the results for He's approach, the albedo estimation errors at SZAs exceeding 70° for the LUT without correction (RMSE = 0.0393, bias = 0.0113, and R^2 = 0.62) decrease significantly compared with the results of He's method (RMSE = 0.0608, bias = 0.0259, and R^2 = 0.35). Regarding the complete data set of 1315 samples, the RMSE after the two-step corrections decreases from 0.0418 to 0.0383 (reduced by 8.37%), and the percentage of biases exceeding 0.05 decreases to from 19.62% to 16.35% (reduced by 16.67%). Significantly, for the results at SZAs exceeding 70°, the RMSE for the postcorrection LUT declines from 0.0608 to 0.0435 (reduced by 28.45%).

In addition, the results at the four homogeneous sites in the SURFRAD network have a higher accuracy for the newly proposed postcorrection LUT (i.e., RMSE = 0.0254).

In summary, using albedo measurements to build and assess the LUT and applying a two-step correction strategy for correcting potential errors not considered by the original direct-estimation albedo algorithm, these improvements show the potential to estimate albedo at high spatial resolutions for near-nadir-viewing sensors. Future efforts should be focused on the cross comparison of the proposed method in this article with several current methods of albedo inversion at the 30-m Landsat scale. Moreover, the recently developed snow BRDF model [51], [52] can be used to improve the accuracy on snow albedo estimation. A more accurate fraction of diffuse irradiance based on measurements or simulations from AODs, SZAs, bands, and aerosol model types [26], [53] is necessary, which may help improve the adjustment accuracy of the MODIS BRDF parameters during the first correction step. In addition, this method may be further investigated for application to other near-nadir-viewing satellites, such as Sentinel 2A.

References

[1] G. B. Bonan, "Forests and climate change: Forcings, feedbacks, and the climate benefits of forests," *Science*, vol. 320, no. 5882, pp. 1444–1449, Jun. 2008.

[2] R. E. Dickinson, "Land processes in climate models," *Remote Sens. Environ.*, vol. 51, no. 1, pp. 27–38, Jan. 1995.

[3] M. J. Barnsley, A. H. Strahler, K. P. Morris, and J.-P. Muller, "Sampling the surface bidirectional reflectance distribution function (BRDF): 1. Evaluation of current and future satellite sensors," *Remote Sens. Rev.*, vol. 8, no. 4, pp. 271–311, pp. 271–311 1994.

[4] J.-L. Roujean, M. Leroy, and P.-Y. Deschamps, "A bidirectional reflectance model of the Earth's surface for the correction of remote sensing data," *J. Geophys. Res., Atmos.*, vol. 97, no. D18, pp. 20455–20468, Dec. 1992.

[5] W. Wanner, X. W. Li, and A. H. Strahler, "On the derivation of kernels for kernel-driven models of bidirectional reflectance," *J. Geophys. Res., Atmos.*, vol. 100, no. D10, pp. 21077–21089, Oct. 1995.

[6] C. B. Schaaf *et al.*, "First operational BRDF, albedo nadir reflectance products from MODIS," *Remote Sens. Environ.*, vol. 83, nos. 1–2, pp. 135–148, Nov. 2002.

[7] D. Carrer, E.S. Bruno Smets, X. Ceamanos, and J. Roujean, *Vegetation and Energy, Algorithm Theoretical Basis Document*, document, Copernicus Global Land Operations-Lot 1, Version 1. Issue I2.11., Feb. 2018.

[8] D. Carrer, E.S. Bruno Smets, X. Ceamanos, and J. Roujean, *Vegetation and Energy, Algorithm Theoretical Basis Document*, document, Copernicus Global Land Operations-Lot 1, Version 1.5. Issue I2.21., Jul. 2018.

[9] Z. Xiao, S. Liang, J. Wang, D. Xie, J. Song, and R. Fensholt, "A framework for consistent estimation of leaf area index, fraction of absorbed photosynthetically active radiation, and surface albedo from MODIS time-series data," *IEEE Trans. Geosci. Remote Sens.*, vol. 53, no. 6, pp. 3178–3197, Jun. 2015.

[10] X. Zhang *et al.*, "Potential investigation of linking PROSAIL with the ross-li BRDF model for vegetation characterization," *Remote Sens.*, vol. 10, no. 3, p. 437, Mar. 2018.

[11] M. O. Roman *et al.*, "Use of *in situ* and airborne multiangle data to assess MODIS- and Landsat-based estimates of directional reflectance and albedo," *IEEE Trans. Geosci. Remote Sens.*, vol. 51, no. 3, pp. 1393–1404, Mar. 2013.

[12] X. Li, F. Gao, J. Wang, and A. Strahler, "A priori knowledge accumulation and its application to linear BRDF model inversion," *J. Geophys. Res., Atmos.*, vol. 106, no. 11, pp. 11925–11935 2001.

[13] B. Franch, E. Vermote, and M. Claverie, "Intercomparison of Landsat albedo retrieval techniques and evaluation against in situ measurements across the US SURFRAD network," *Remote Sens. Environ.*, vol. 152, pp. 627–637, Sep. 2014.

[14] Y. Shuai, J. Masek, F. Gao, and C. B. Schaaf, "An algorithm for the retrieval of 30-m snow-free albedo from Landsat surface reflectance and MODIS BRDF," *Remote Sens. Environ.*, vol. 115, no. 9, pp. 2204–2216, Apr. 2011.

[15] Z. Jiao, H. Zhang, Y. Dong, Q. Liu, Q. Xiao, and X.W. Li, "An algorithm for retrieval of surface albedo from small view-angle airborne observations through the use of BRDF archetypes as prior knowledge," *IEEE J. Sel. Topics Appl. Earth Observat. Remote Sens.*, vol. 8, no. 7, pp. 3279–3293, Jul. 2015.

[16] J. G. Masek *et al.*, "A Landsat surface reflectance dataset for North America, 1990-2000," *IEEE Geosci. Remote Sens. Lett.*, vol. 3, no. 1, pp. 68–72, Jan. 2006.

[17] Y. Shuai, J. G. Masek, F. Gao, C. B. Schaaf, and T. He, "An approach for the long-term 30-m land surface snow-free albedo retrieval from historic Landsat surface reflectance and MODIS-based a priori anisotropy knowledge," *Remote Sens. Environ.*, vol. 152, pp. 467–479, Jul. 2014.

[18] D. P. Roy *et al.*, "Landsat-8: Science and product vision for terrestrial global change research," *Remote Sens. Environ.*, vol. 145, pp. 154–172, Apr. 2014.

[19] E. Vermote, C. O. Justice, and F.-M. Breon, "Towards a generalized approach for correction of the BRDF effect in MODIS directional reflectances," *IEEE Trans. Geosci. Remote Sens.*, vol. 47, no. 3, pp. 898–908, Mar. 2009.

[20] B. Tan *et al.*, "The impact of gridding artifacts on the local spatial properties of MODIS data: Implications for validation, compositing, and band-to-band registration across resolutions," *Remote Sens. Environ.*, vol. 105, no. 2, pp. 98–114, Nov. 2006.

[21] S. Sandmeier, C. Müller, B. Hosgood, and G. Andreoli, "Sensitivity analysis and quality assessment of laboratory BRDF data," *Remote Sens. Environ.*, vol. 64, no. 2, pp. 176–191, May 1998.

[22] T. He, S. Liang, D. Wang, X. Chen, D.-X. Song, and B. Jiang, "Land surface albedo estimation from Chinese HJ satellite data based on the direct estimation approach," *Remote Sens.*, vol. 7, no. 5, pp. 5495–5510, May 2015.

[23] T. He, S. Liang, D. Wang, Y. Cao, F. Gao, Y. Yu, and M. Feng, "Evaluating land surface albedo estimation from Landsat MSS, TM, ETM+, and OLI data based on the unified direct estimation approach," *Remote Sens. Environ.*, vol. 204, pp. 181–196, Jan. 2018.

[24] S. Liang, "A direct algorithm for estimating land surface broadband albedos from MODIS imagery," *IEEE Trans. Geosci. Remote Sens.*, vol. 41, no. 1, pp. 136–145, Jan. 2003.

[25] S. Liang, A. H. Strahler, and C. Walthall, "Retrieval of land surface albedo from satellite observations: A simulation study," *J. Appl. Meteorol.*, vol. 38, no. 6, pp. 712–725, Jun. 1999.

[26] Y. Qu, Q. Liu, S. Liang, L. Wang, N. Liu, and S. Liu, "Direct-estimation algorithm for mapping daily land-surface broadband albedo from MODIS data," *IEEE Trans. Geosci. Remote Sens.*, vol. 52, no. 2, pp. 907–919, Feb. 2014.

[27] S. Liang *et al.*, "A long-term Global LAnd Surface Satellite (GLASS) data-set for environmental studies," *Int. J. Digit. Earth*, vol. 6, no. 1, pp. 5–33, Dec. 2013.

[28] D. Wang, S. Liang, T. He, and Y. Yu, "Direct estimation of land surface albedo from VIIRS data: Algorithm improvement and preliminary validation," *J. Geophys. Res., Atmos.*, vol. 118, no. 22, pp. 577–586, Nov. 2013.

[29] C. O. Justice *et al.*, "Land and cryosphere products from Suomi NPP VIIRS: Overview and status," *J. Geophys. Res., Atmos.*, vol. 118, no. 17, pp. 9753–9765, Sep. 2013.

[30] D. Wang, S. Liang, Y. Zhou, T. He, and Y. Yu, "A new method for retrieving daily land surface albedo from VIIRS data," *IEEE Trans. Geosci. Remote Sens.*, vol. 55, no. 3, pp. 1765–1775, Mar. 2017.

[31] J. Ju, D. Roy, E. Vermote, J. Masek, and V. Kovalskyy, "Continental-scale validation of MODIS-based and LEDAPS Landsat ETM+ atmospheric correction methods," *Remote Sens. Environ.*, vol. 122, pp. 175–184, Jul. 2012.

[32] Z. Wang *et al.*, "Evaluation of MODIS albedo product (MCD43A) over grassland, agriculture and forest surface types during dormant and snow-covered periods," *Remote Sens. Environ.*, vol. 140, pp. 60–77, Jan. 2014.

[33] J. Liu *et al.*, "Validation of Moderate Resolution Imaging Spectroradiometer (MODIS) albedo retrieval algorithm: Dependence of albedo on solar zenith angle," *J. Geophys. Res., Atmos.*, vol. 114, no. D1, pp. 1–11, Jan. 2009.

[34] Y. Jin *et al.*, "Consistency of MODIS surface bidirectional reflectance distribution function and albedo retrievals: 2. Validation," *J. Geophys. Res., Atmos.*, vol. 108, no. D5, p. 4159, Mar. 2003.

[35] D. P. Roy *et al.*, "A general method to normalize Landsat reflectance data to nadir BRDF adjusted reflectance," *Remote Sens. Environ.*, vol. 176, pp. 255–271, Apr. 2016.

[36] Z. Jiao *et al.*, "The influence of spatial resolution on the angular variation patterns of optical reflectance as retrieved from MODIS and POLDER measurements," *Remote Sens. Environ.*, vol. 215, no. 9, pp. 371–385, Sep. 2018.

[37] L. Bai, X. Huang, Z. Wu, and L. Guo, "The scale effects of anisotropic land surface reflectance: An analysis with Landsat and MODIS imagery," *Proc. SPIE*, vol. 9646, Oct. 2015, Art. no. 96460W.

[38] M. O. Román, C. K. Gatebe, C. B. Schaaf, R. Poudyal, Z. Wang, and M. D. King, "Variability in surface BRDF at different spatial scales (30 m–500 m) over a mixed agricultural landscape as retrieved from airborne and satellite spectral measurements," *Remote Sens. Environ.*, vol. 115, no. 9, pp. 2184–2203, Sep. 2011.

[39] Z. Wang *et al.*, "Monitoring land surface albedo and vegetation dynamics using high spatial and temporal resolution synthetic time series from Landsat and the MODIS BRDF/NBAR/albedo product," *Int. J. Appl. Earth Observ. Geoinf.*, vol. 59, pp. 104–117, Jul. 2017.

[40] C. B. Schaaf, J. Liu, F. Gao, and A. H. Strahler, "Aqua and Terra MODIS albedo and reflectance anisotropy products," *Land Remote Sensing and Global Environmental Change: NASA's Earth Observing System and the Science of ASTER and MODIS*, B. Ramachandran, C. O. Justice, and M. J. Abrams Eds. New York, NY, USA: Springer, 2011, pp. 549–561.

[41] A. Cescatti *et al.*, "Intercomparison of MODIS albedo retrievals and in situ measurements across the global FLUXNET network," *Remote Sens. Environ.*, vol. 121, pp. 323–334, Jun. 2012.

[42] W. Lucht, C. B. Schaaf, and A. H. Strahler, "An algorithm for the retrieval of albedo from space using semiempirical BRDF models," *IEEE Trans. Geosci. Remote Sens.*, vol. 38, no. 22, pp. 977–998, Mar. 2000.

[43] Y. Shuai *et al.*, "Daily MODIS 500 m reflectance anisotropy direct broadcast (DB) products for monitoring vegetation phenology dynamics," *Int. J. Remote Sens.*, vol. 34, no. 16, pp. 5997–6016, Aug. 2013.

[44] Z. Jiao *et al.*, "A method for improving hotspot directional signatures in BRDF models used for MODIS," *Remote Sens. Environ.*, vol. 186, pp. 135–151, Dec. 2016.

[45] W. Lucht and P. Lewis, "Theoretical noise sensitivity of BRDF and albedo retrieval from the EOS-MODIS and MISR sensors with respect to angular sampling," *Int. J. Remote Sens.*, vol. 21, no. 1, pp. 81–98, Jan. 2000.

[46] X. Li and A. H. Strahler, "Geometric-optical bidirectional reflectance modeling of the discrete crown vegetation canopy: Effect of crown shape and mutual shadowing," *IEEE Trans. Geosci. Remote Sens.*, vol. 30, no. 2, pp. 276–292, Mar. 1992.

[47] Z. Jiao, M. J. Hill, C. B. Schaaf, H. Zhang, Z. Wang, and X. Li, "An anisotropic flat index (AFX) to derive BRDF archetypes from MODIS," *Remote Sens. Environ.*, vol. 141, pp. 168–187, Feb. 2014.

[48] W. Qin, J. R. Herman, and Z. Ahmad, "A fast, accurate algorithm to account for non-Lambertian surface effects on TOA radiance," *J. Geophys. Res., Atmos.*, vol. 106, no. D19, pp. 22671–22684, Oct. 2001.

[49] N. C. Strugnell and W. W. Lucht, "An algorithm to infer continental-scale albedo from AVHRR data, land cover class, and field observations of typical BRDFs," *J. Climate*, vol. 14, no. 7, pp. 1360–1376 2001.

[50] S. Liang, "Narrowband to broadband conversions of land surface albedo I: Algorithms," *Remote Sens. Environ.*, vol. 76, no. 2, pp. 213–238, May 2001.

[51] Z. Jiao *et al.*, "Development of a snow kernel to better model the anisotropic reflectance of pure snow in a kernel-driven BRDF model framework," *Remote Sens. Environ.*, vol. 221, pp. 198–209, Feb. 2019.

[52] A. Ding *et al.*, "An assessment of the performance of two snow kernels in characterizing snow scattering properties," *Int. J. Remote Sens.*, vol. 40, no. 16, pp. 6315–6335, Mar. 2019.

[53] Y. Dong *et al.*, "A modified version of the kernel-driven model for correcting the diffuse light of ground multi-angular measurements," *Remote Sens. Environ.*, vol. 210, pp. 325–344 Jun. 2018.

Xiaoning Zhang received the B.E. degree in surveying and mapping from the China University of Mining and Technology, Beijing, China, in 2014, and the Ph.D. degree in GIS from Beijing Normal University, Beijing, in 2019.

She is currently an Engineer with the Unmanned Aerial Vehicle Systems Engineering Institute, China Aerospace Science and Technology Corporation, Beijing. Her research interests include albedo retrieving and validation, scale effect of bidirectional reflectance distribution function (BRDF), and the quantitative inversion of vegetation parameters based on BRDF data and radiative transfer theory.

Ziti Jiao received the B.Sc. degree in mining engineering from the Wuhan Institute of Technology, Wuhan, China, in 1993, the M.Sc. degree from the School of Geography, Beijing Normal University (BNU), Beijing, China, in 2002, the Ph.D. degree in geographic information system from BNU in 2008, and the Ph.D. degree in remote sensing from Boston University (BU), Boston, MA, USA, in 2009.

He attended the exchange program between BNU and BU in 2004. He is currently a Professor with the Institute of Remote Sensing Science and Engineering, Faculty of Geographical Science, BNU. He is involved in the development of the operational clumping index (CI) products to monitor the Earth's environments using the multiangle signatures. He has been focusing on the development of the kernel-driven bidirectional reflectance distribution function (BRDF) models, including modeling hotspot effect and snow scattering optics in the kernel-driven BRDF model framework. His research interests include modeling reflectance anisotropy and albedo using remotely sensed data to monitor the reflectance characteristics of various land surfaces.

Dr. Jiao is currently the Editorial Board Member of *Remote Sensing*. He serves as a Reviewer for *Remote Sensing of Environment* and the IEEE TRANSACTIONS ON GEOSCIENCE AND REMOTE SENSING.

Yadong Dong received the B.S., M.S., and Ph.D. degrees in cartography and geography information systems from the School of Geography, Beijing Normal University, Beijing, China, in 2011, 2014, and 2017, respectively.

He has finished the Post-Doctoral Research with Beijing Normal University in 2019. He is currently a Research Assistant with the Institute of Remote Sensing and Digital Earth, Chinese Academy of Sciences, Beijing. His research interests include the improvement of the kernel-driven model and its application in estimating clumping index.

ZHANG *et al.*: DEVELOPMENT OF THE DIRECT-ESTIMATION ALBEDO ALGORITHM FOR SNOW-FREE LANDSAT TM ALBEDO RETRIEVALS

Tao He received the B.E. degree in photogrammetry and remote sensing from Wuhan University, Wuhan, China, in 2006, and the Ph.D. degree in geography from the University of Maryland, College Park, MD, USA, in 2012.

He is currently a Professor with the School of Remote Sensing and Information Engineering, Wuhan University, and the Department of Geographical Sciences, University of Maryland. His research interests include surface anisotropy and albedo modeling, data fusion of satellite products, and long-term regional and global surface radiation budget analysis.

Anxin Ding received the B.S. degree from the Anhui University of Science and Technology, Huainan, Anhui, China, in 2016, and the M.S. degree from Beijing Normal University, Beijing, China. He is currently pursuing the Ph.D. degree with Wuhan University, Wuhan, China.

His research interests include Ross-Thick-Li-Sparse-Reciprocal (RTLSR) model and snow bidirectional reflectance distribution function (BRDF) model, and snow albedo.

Siyang Yin received the M.E. degree in surveying and mapping engineering from the Institute of Remote Sensing and Digital Earth, Chinese Academy of Science, Beijing, China, in 2017. She is currently pursuing the Ph.D. degree with Beijing Normal University, Beijing.

Her research interests include production and analysis of clumping index data and representative assessment of field data.

Hu Zhang received the B.S. degree from Shandong Jianzhu University, Jinan, Shandong, China, in 2009, and the M.S. and Ph.D. degrees in geography from Beijing Normal University, Beijing, China, in 2012 and 2015.

He is currently a Lecturer with the School of Geographic and Environmental Sciences, Tianjin Normal University, Tianjin, China. His research interests include land surface reflectance anisotropy classification and land surface albedo retrieval based on prior knowledge.

Lei Cui received the B.S. degree from the Xiamen University of Technology, Xiamen, China, in 2014. He is currently pursuing the Ph.D. degree with Beijing Normal University, Beijing, China.

His research interests include inversion of vegetation structure parameters based on waveform LIDAR data and multiangle remote sensing data.

Yaxuan Chang received the B.S. degree in geographic information science from Northeast Forest University, Harbin, China, in 2017. She is currently pursuing the master's degree with Beijing Normal University, Beijing, China.

Her research interests include the kernel-driven model and the calibration of hotspot parameters of these models based on bidirectional reflectance distribution function (BRDF) data and radiative transfer theory.

Jing Guo received the B.S. degree in geographic information science from Northeast Forestry University, Harbin, China, in 2018. She is currently pursuing the master's degree with Beijing Normal University, Beijing, China.

Her research interests include the kernel-driven model and snow bidirectional reflectance distribution function (BRDF) model.

Rui Xie received the B.S. degree from the Shandong University of Science and Technology, Qingdao, China, in 2018. She is currently pursuing the master's degree with Beijing Normal University, Beijing, China.

Her research interest includes the analysis and statistics of clumping index (CI) products.

Authorized licensed use limited to: Beijing Normal University. Downloaded on March 11,2020 at 13:13:27 UTC from IEEE Xplore. Restrictions apply.